Ultracold atoms experiment for trapping ^{39}K in an optical box trap.

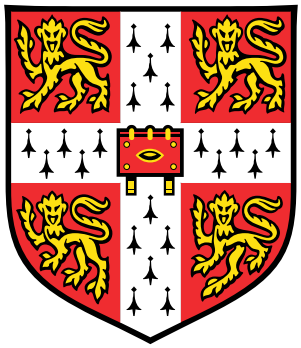

Aziza Suleymanzade

Department of Physics

University of Cambridge

This dissertation is submitted for the degree of Master of Philosophy

Master of Philosophy

Emmanuel College

2014

Declaration

This dissertation is the result of my own work and includes nothing which is the outcome of work done in collaboration except where specifically indicated in the text

Aziza Suleymanzade
2014

Acknowledgements

Over the course of the year, I received help and advice from number of people, who I would like to acknowledge. I would like to thank Zoran Hadzibabic and Robert Smith, who both helped in supervising my work this year. In addition at various times I was benefitted by the contributions from the other members of our AMOP group (Alex Gaunt, Richard Fletcher, Nir Navon, Igor Gotlibovich, Tobias Schmutz and Martin Robert-de-Saint-Vincent). Finally, I would also like to acknowledge the work performed by Sarah Thomas and Yago V-I. Redondo in helping to setup the Laser System.

Contents

1

Introduction

Many-body quantum systems is one of the most active fields of study in modern physics. Since the rise of quantum mechanics (QM) in the early twentieth century theoretical aspects of this profound theory have been widely researched. However, experimental investigations were far out of reach due to a lack of appropriate tools. It wasn't until the first practical realizations of the laser in 1960s that the field of many-body physics started showing hope for experimental research, after all, laser light itself is a coherent system of photon. Of course, there have been a lot of studies on bulk materials and their QM characteristics in experimental condensed matter physics. But these systems are notoriously complex and difficult to control. Only with great advances in the field of cold atoms and the first in-lab Bose-Einstein condensate (BEC), a quantum degenerate gas created in 1995 [2, 9], did direct experimental control of many-body quantum systems become available.

Degenerate cold gases, such as BEC, not only give us an opportunity to study the quantum phenomena in cold atoms systems, but also give a unique means to experimentally simulate a diverse range of other many-body quantum systems. These simulations are not possible otherwise since underlying QM behavior is very hard to translate efficiently into the classical language of conventional computers. The robust nature and unprecedented level of control of both internal (electronic) and external (motional) degrees of freedom that cold atoms provide make them a great tool for investigating complex quantum dynamics. We are reaching a point where we can fabricate in the lab any Hamiltonian of the form:

$$H = \underbrace{H_{\text{int}}}_{\text{Interaction}} + \underbrace{H_{\text{pot}}}_{\text{Potential}} + \underbrace{H_{\text{kin}}}_{\text{Kinetic}} . \tag{1.1}$$

We can manipulate H_{int} - the interaction energy of the system, H_{pot} - the potential energy and H_{kin} - a kinetic energy, using magnetic and optical methods.

Behind every groundbreaking research in the field of cold atoms, there is a sophisticated experimental setup creating and manipulating the quantum degenerate gasses. In the past two decades this field has greatly advanced. New ways of trapping and cooling atoms have been implemented that improved the efficiency of creating degenerate gases. By now scientists have condensed over 16 different atomic species, summarized in Table B.1 of Appendix A. Each species, due to its unique structure, provides a new insight and opportunity for novel manipulation methods.

In this thesis I will be talking about ^{39}K, which is central to our experiment. From the Hamiltonian perspective (1.1), ^{39}K gives us ability to tune the interaction between atoms, H_{int}, with high precision through its Feshbach resonances [12, 23]. Different potentials that atoms occupy after condensation determine H_{pot}. In the past, the most popular potentials have been the harmonic trap and optical lattices in various dimensions due to their practical ease. But with advances in Spatial Light Modulators (SLMs) it is now possible to create an optical trap essentially of any shape. The potential we will be using for this setup is a uniform box. Our group recently demonstrated the first three-dimensional BEC in a uniform potential using an SLM [19]. This was a long-sought realization of the uniform Bose gas so familiar from statistical mechanics textbooks.

In this thesis I will discuss a new ^{39}K BEC machine, that I have been building as my MPhil project, with a uniform box potential. It follows the design of our previous potassium BEC machine with small alterations. It will incorporate our group's past successes with tunable interactions of ^{39}K and new physics of a cold atoms in a uniform potential that has not been experimentally accessible before.

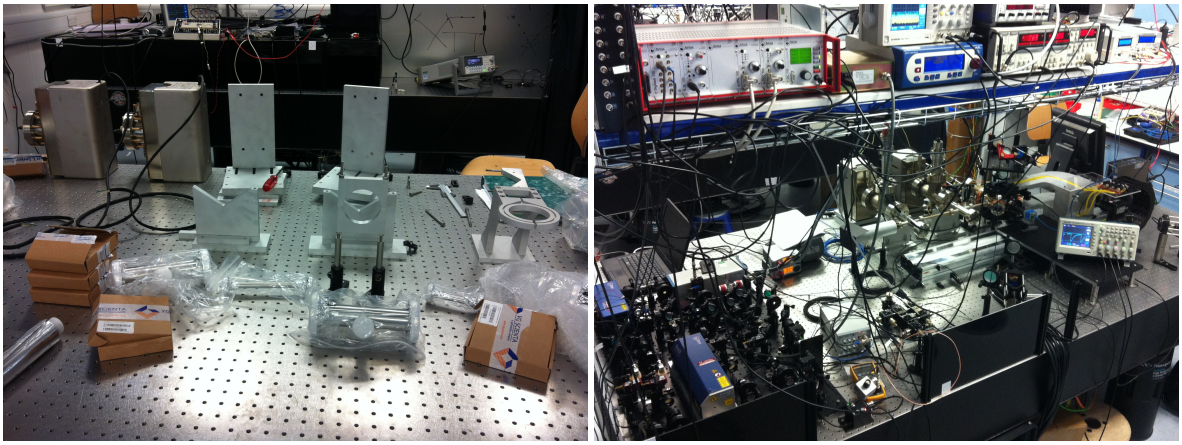

Fig. 1.1 Optical table: to the left - on 03/10/2013, to the right - on 06/05/2014

1.1 BEC

Degenerate cold gases have been used to study systems of both composite fermions (Fermi gas) and bosons (BEC). Fermions, with half-integer spin, and bosons, with integer spins, are the two fundamental types of matter that make up the world. In the classical regime both fermions and bosons act exactly the same - as distinguishable objects making up a thermal gas. However, when we get large number of atoms together in the quantum regime, the intrinsically different statistics that underly their behavior bring out very different collective quantum phenomena. Fermions, due to the Pauli exclusion principle, tend to avoid each other regardless of the phase-space density, whereas bosons collapse into one state under a phase transition. In our lab we work with bosons and BEC as our many-body quantum simulator.

BEC is essentially a new state of matter with peculiar properties. The phase transition from a classical gas into a degenerate quantum regime is very unique. Usually, transitions between states of matter, like gas and liquid, occur due to a change in interaction strength between particles as we change thermodynamic parameters. But the BEC transition is purely statistical and occurs even in the absence of interactions. The main concept behind the BEC transition is that as we lower the thermal energy $k_{\mathrm{B}}T$ of atoms in comparison to the energy spacings of the system, bosons find it more energy-efficient to collectively jump into the ground state. This creates a coherent many-body quantum system from a thermal classical gas. The effect was first theoretically predicted by Einstein in 1925 [13].

As simple as this behavior sounds, we don't usually observe it in the world for two reasons. One is that only bosons are comfortable enough with each other to occupy the same state (it would never happen to fermions). The second, most important, reason is that the temperatures at which BEC occurs are extremely low. The temperature needs to be sufficiently low for the de Broglie wavelength of particles to reach the size of the inter-particle distances. The issue is that these distances have to be quite large in order to avoid three body recombinations and other destructive effects of atomic interactions. As a result the cold atomic gases are extremely dilute, up to 10^6 times more dilute than air. Only then, in the quantum regime, does the indistinguishable bosonic behavior emerge. The thermal de Broglie wavelength of an atom, that quantifies the spread of the atomic wave function, is

$$\lambda_{\mathrm{T}} = \sqrt{\frac{2\pi\hbar^2}{mk_{\mathrm{B}}T}}.$$

In a three dimensional gas with particle density n, the average distance between atoms is $\sim n^{-\frac{1}{3}}$. Therefore, the BEC phase transition occurs at the point where the phase-space density

is approximately equal to 1:

$$\rho = n\lambda_T^3 \approx 1$$

.

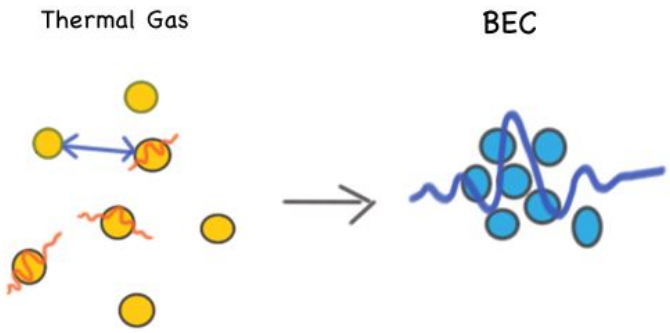

Fig. 1.2 Illustration of the phase transition from the classical thermal gas to BEC.

As an example, for an ideal gas of 10^7 ^{39}K atoms in a uniform box of dimensions $(95 \times 95 \times 95)\mu$m a rough estimate of average inter particle distance is 0.4 μm. This means, in order to create a BEC, atoms need to be at about 400 nK. To emphasize the extremity of this regime a temperature scale is shown in Figure 1.3 for a relative comparison.

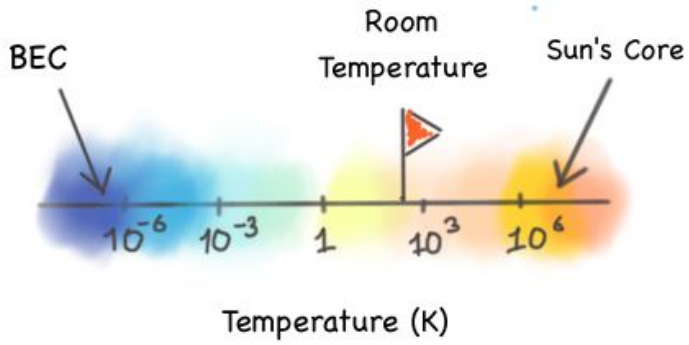

Fig. 1.3 Relative temperature comparison of the BEC transition to the room temperature and temperature at the sun's core

1.2 Potassium 39

In our lab we mainly work with ^{39}K atoms, which is the most naturally abundant bosonic isotope of potassium. Some of the ^{39}K properties are summarized in Table 1.1.

Electronic structure	$1s^2 2s^2 p^6 4s^1$
Mass (u) [4]	38.96370668(20)
Nuclear spin	$3/2$
Main Optical transitions	D1 line: $^2S_{1/2} \rightarrow ^2P_{1/2}$ D2 line: $^2S_{1/2} \rightarrow ^2P_{3/2}$

Table 1.1 Properties of ^{39}K

The choice of atomic species greatly affects the experimental setup. Amongst previously condensed atoms ^{39}K is not the easiest choice for the experiment. Its poorly resolved hyperfine structure makes it a very difficult to cool. The conventional cooling methods, such as *optical molasses* and *Sisyphus cooling*, that work so well on ^{87}Rb atoms are not efficient for cooling potassium atoms below the *sub-Doppler temperature limit*. The relatively small background scattering length of ^{39}K makes *evaporative cooling* less efficient. Finally, the fact that the background interaction strength is attractive for ^{39}K results in an instability of the BEC. We solved the issue of ineffective cooling by introducing sub-Doppler cooling methods using the D1 line. And the last two difficulties were eliminated using one of the most attractive features of ^{39}K - Feshbach resonances, through which we can alter both the sign and absolute value of the scattering length.

In spite of the relative challenges connected to cooling and condensing, working with ^{39}K atoms has many advantages. First of all, there are other bosonic and fermionic isotopes such as ^{40}K and ^{41}K, that have been condensed, the properties of which are well known. This opens a possibility to study mixtures of ultra-cold gases. Also, the commercial lasers of suitable frequencies for ^{39}K are readily available for purchase. Most importantly, the existence of several Feshbach resonances of ^{39}K atoms as well as interspecies ^{39}K - ^{87}Rb, ^{41}K -^{87}K resonances at moderate magnetic fields allows us to tune interactions between atoms, H_{int}, and study quantum many-body systems at various interaction regimes.

1.3 Use of D1 light in Cooling ^{39}K

As was mentioned before, the poor resolution of the hyperfine structure of ^{39}K results in inefficient sub-Doppler cooling using conventional the molasses technique with the D2 line. Because of this we decided to try a new cooling technique using a D1 line, called gray molasses. The theory behind this mechanism was discovered in 1990s [43], since then it has been used for cooling various atomic species, including ^{133}Cs atoms to 1.1 μK in 1996 [5], ^{7}Li atoms to 60 μ K in 2013 [21] and ^{40}K atoms to 20 μ K in 2012 [15]. The most recent two papers by G. Salomon et al and Nath et al have demonstrated the same effect in ^{39}K, cooling the atoms down to 6 μ K [34] and 12 μ K [29] respectively.

The gray molasses (GM) cooling technique combines the *velocity-dependent population transfer* between *dark states* and *bright states* and Sisyphus cooling. Due to limited capture velocity, before the GM step it is necessary to pre-cool the cloud, either using conventional D2 molasses or using the compressed MOT with the D1 light. The mechanism of the cooling sequence will be discussed in details in Chapter 4.

1.4 Uniform Box

To manipulate the potential energy of a many-body system, H_{int}, we use flexible geometries of an optical trap provided by a spatial light modulator. An SLM allows us to create custom optical traps for atoms of various shapes and dimensions. This flexibility opens a window for experimental investigations of various physical systems.

Our group's previous effort in working with versatile optical traps inspired the creation of the simplest one - a uniform box potential. Theoretically, it is the most common potential because of its abundance and simplicity. However, experimentally it has always been out of reach due to practical difficulties of its realization. In 2013 our group created the first ever BEC (of ^{87}Rb) in a three-dimensional homogeneous potential [19]. Inspired by this the success, it was decided that the new ^{39}K system will incorporate the uniform box potential as one of its features.

1.5 Research Goals

Previously in the lab we had two BEC machines, one producing a ^{87}Rb BEC in a uniform potential and another one producing ^{39}K BEC with tunable interactions in a harmonic trap. The new system incorporates these features providing a new more powerful toolset for future

research. A few of the many systems and phenomena that would be interesting and possible to study are:

- **Non-interacting BEC in a Uniform Box Potential.** A truly classic example of a text-book BEC, that hasn't been experimentally realized before - the ideal uniform Bose gas. In theory it should acquire a gaussian shape in a uniform potential. In the ^{87}Rb case, which has fixed non-zero interaction strength, atoms push each other away which results in deviation from gaussian-shaped cloud in a uniform potential.

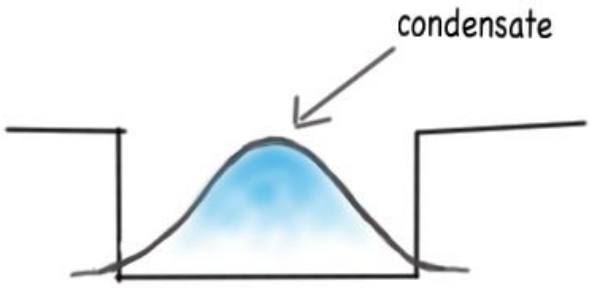

Fig. 1.4 Non-Interacting BEC in a Uniform Box potential

- **BEC at a unitary limit.** For a gas with infinite Interaction strengths between atoms ($a \to \infty$) theoretical descriptions breakdown. This is one of the reasons why experimental pursuit of the unitary regime has been very active [16]. It is expected for a strongly interacting gas in a uniform potential to acquire the shape of the box due to the extreme repulsion between atoms.

- **T_c shift with interaction strengths.** Our group has studied effects of interactions on the critical temperature of a BEC in a harmonic trap [35]. It would be very interesting to study these effects in a box potential, considering the theoretical predictions are much simpler for a uniform BEC.

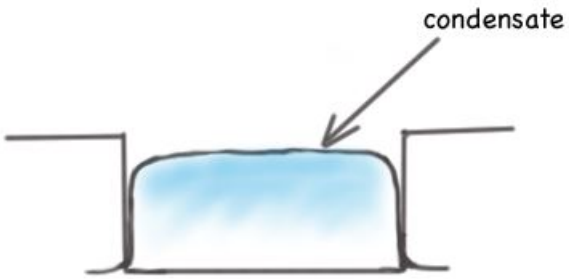

Fig. 1.5 Unitary BEC in a Uniform Box potential

1.6 Outline

In the rest of the thesis I will discuss theoretical background and experimental details of various stages of building the new ^{39}K BEC machine:

- **Chapter 2 Vacuum System**
- **Chapter 3 Theory of Laser Cooling**
- **Chapter 4 Laser System**
- **Chapter 5 Current Work**
- **Chapter 6 Conclusion**
- **Appendices A and B**

2

Vacuum System

The creation of a suitable environment for cold atoms is an involved task, since the atomic gases need to be dilute and isolated from any unwanted perturbations. Usually, the experiment takes place in stainless steel chambers. During the sequence atoms are transferred from one field trap to another suspended in a vacuum. This keeps them from interacting with any solid surfaces. One of the characteristics of a good experimental setup in our field is a long lifetime of the atomic cloud. Lifetimes on the order of minutes are optimal for research. The main process that limits the lifetime is collisions between atoms and a background vapor in the chamber. To reduce this problem the system must be kept at an ultra-high vacuum (UHV) regime. Pressures less than 10^{-11} mbar are ideal for good performance. In this chapter I will discuss the steps we took to get UHV in our system.

2.1 Overview of the system

The new system is the third BEC experiment built in our lab. It was decided to build it following the design of our currently running ^{39}K machine, since it has been successful for several years and our group had previous experience designing and constructing it. There have been a few modifications. We left out a viewing cube, which is a small cubic chamber with windows on each face, in between the two chambers and pressure gauges due to the previously observed lack of functionality. We have also added a viewpoint at the chamber with atom sources as an extra optical access to the MOT.

Figure 2.1 shows the complete vacuum system and highlights main functional parts. Some of these parts are off-the-shelf pieces while others are custom-made to fit the design of our system. The main material of the chambers is *316LN stainless steel*. The relatively low magnetic susceptibility of this material minimizes stray magnetic fields in our systems.

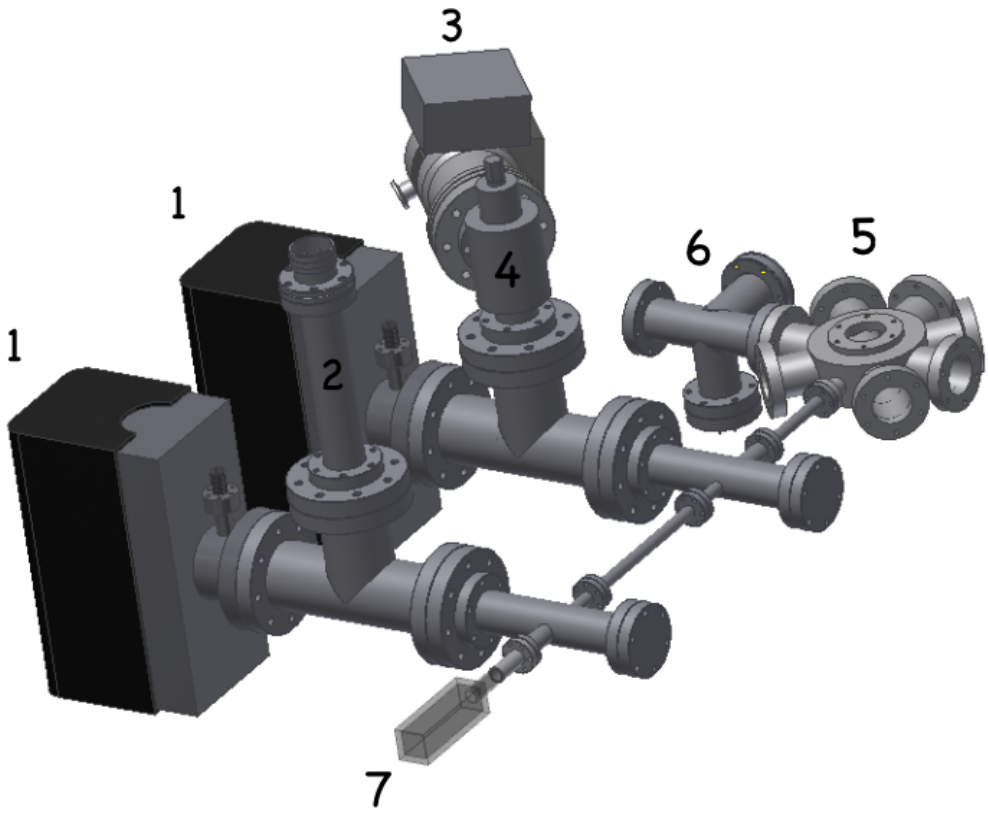

Fig. 2.1 Overview of the system: 1. Ion pumps. 2. Titanium Sublimation pumps. 3. Turbomolecular pump. 4. All-metal right-angle valve. 5. MOT cell. 6. Atom sources. 7. Science cell.

2.1.1 Pumps

We use four different types of pumps at various stages of achieving and maintaining a UHV. The two *Gamma Vacuum TiTan 75S* ion pumps, essential for reaching a UHV regime, work continuously through the lifetime of the system. The pumps function by ionizing the gas and using an electric field to attract charged particles towards the solid electrodes that trap them by chemisorption. Since no particles escape the system through this method they can operate in an environment that is sealed from the air. To have a reasonable lifetime, ion pumps must operate below 10^{-6} mbar.

In preparation for the Ion pumps, the pressure in the system is reduced using an *Oerlikon Leybold Turbovac TW70 H* turbomolecular pump. The turbo pump is only efficient below 20 mbar. That is why we back it up with an *Oerlikon Leybold SC 5 D* scroll pump while the system is still exposed to air. To protect ion pumps from over-contamination we kept the turbo pump on through *baking* (see 2.4) as a support during water vapor releases, even

though on average the pressure was low enough. After a 10^{-9} mbar range was reached, the turbo pump was isolated from the system by sealing the VAT all-metal right-angle valve. During system's operation Ion pumps are supplemented by a *Varian 916-0050* series titanium sublimation pump. It operates by coating the walls of the chamber with a reactive Ti layer that chemically removes molecules such as H_2, which are difficult for the Ion pumps to eliminate. The sublimation pump is turned on, occasionally, by applying a current of 47 A for 1.5 mins to renew the chemically active surface.

2.1.2 Main chambers

The system has two chambers: MOT and science cell as shown on Figure 2.2. In the MOT chamber atoms are captured for the first time in a Magneto-Optical Trap (MOT) and undergo the initial part of the cooling sequence before they are transferred to the second stage. The MOT chamber is made of *316LN* stainless steel and has eight windows to provide optical access for laser beams. The *Parker 406XR* translation stage is used to physically transfer the atoms in a magnetic trap from the MOT to the science cell. The second and final stage of the experiment takes place in the Science Cell, which is a high-quality glass cell from *Starna Scientific*. It is smaller in size - $30 \times 30 \times 110$ mm with 5 mm thick quartz walls which are AR coated on the outside. This configuration allows for close-proximity lenses that are necessary for high-resolution images and increased access for various other lasers and surrounding magnetic coils.

The main reason for two chamber vacuum system is to allow differential pumping between them. At the science cell it is crucial to have the lowest possible pressure, since it hosts the final stage of the experiment. The lifetime of the atoms here determine the quality of the whole setup. At the MOT side a UHV is still required, but the pressure needs to be high enough for a fast loading of atoms from the background vapor. The main idea behind differential pumping is analogous to the potential divider electrical circuit, where voltages are substituted by pressures and electrical conductances by conductances of vacuum tubes. By picking connector tubes of particular conductance ratio, it is possible to achieve a corresponding ratio of pressures in the chambers they lead to. In our system the ratio of over 100 is achieved between the MOT and the science cell. The more details of the differential pumping design can be found in the PhD theses of Naaman Tammuz and Robbie Campbell [7, 39].

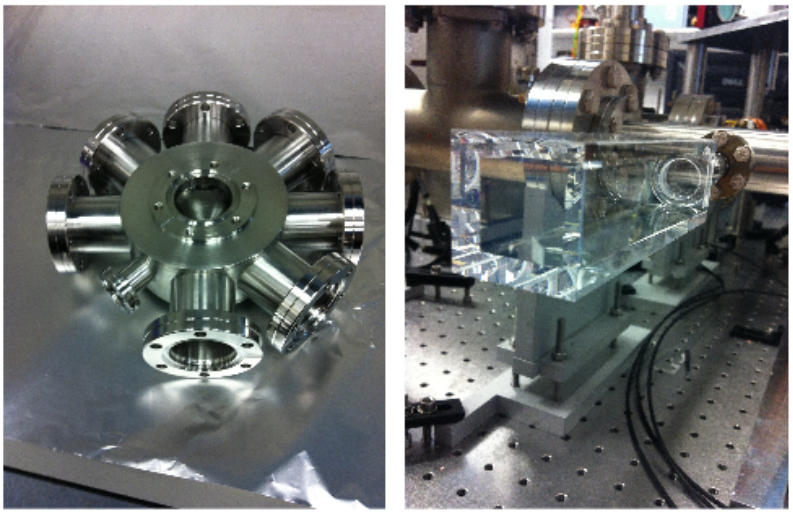

Fig. 2.2 On the left: the MOT chamber. On the right: the science cell.

2.1.3 Atom Sources

The UHV in the system is kept by sealing off the vacuum chambers from the environment. Since the machine doesn't include the valve between the chamber with sources and the MOT, the choice of atom sources had to be made far in advance. It was decided to use four sources: K, ^{40}K, Rb, ^{87}Rb) from *Alvatec*. K and Rb sources provide all the respective naturally occurring isotopes as shown in Table 2.1. Enriched ^{40}K and ^{87}Rb sources produce concentrated amounts of the particular isotope. These sources are based on an alloy of the alkali metal and have an indium seal which allows for exposure to air during the assembly of the system. Above the indium melting point, 160 °C, the sources are fully functional and cannot be exposed to the air due to oxidation. To release atoms a 5-6 A current is passed through the contacts for 1-2 min. The sources are spot welded to contacts on a UHV electrical feedthrough, allowing external electrical access as shown in Figure 2.3.

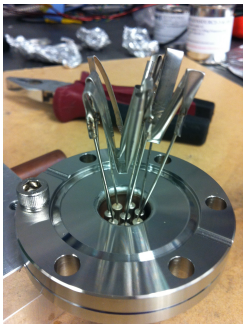

Fig. 2.3 Atom sources spot welded to the UHV electrical feedthrough

Isotope	Natural Abundance (%)
^{85}Rb	72.17
^{87}Rb	27.83
^{39}K	93.26
^{40}K	0.012
^{41}K	6.73

Table 2.1 Natural abundances of the isotopes of rubidium and potassium

At this stage of the experiment it is enough to fire atoms once in 24 hours, but in the future the frequency might change. Rubidium and potassium are convenient species due to their relatively high vapor pressure at room temperature, 4×10^{-7} mbar and 2×10^{-8} mbar respectively. This means we can load the MOT straight from the coating layer that covers the walls of the MOT after the sources have been fired.

2.2 Cleaning

Before the assembly most of the parts have been thoroughly cleaned even though they were all brand new. The chamber parts were either cleaned by hand with acetone or by immersion in acetone in an ultrasonic bath. Clean nitrile gloves were worn at all times to avoid leaving any dirt or fingerprints. After acetone the parts were rinsed with isopropanol since it evaporates much quicker than acetone, leaving less residue. The viewports were cleaned with methanol to avoid damage to the AR coating. At the end of the cleaning procedure all of the items were wrapped in clean aluminum foil until the assembly to avoid further contaminations as shown in Figure 2.4

Fig. 2.4 On the left: the vacuum system part immersed in an acetone ultrasonic bath. On the right: the parts, wrapped in aluminum foil, laid down on the table after cleaning.

2.3 Assembly

All of the necessary parts were laid out in the correct order prior to assembly. Following the cleaning procedure parts have been put together while wearing nitrile gloves. During the construction CF flanges were inspected for any damage and wiped with methanol. The separate items of the chamber were joined by non-reusable copper gaskets, through a sharp knife edge on each pair of flanges. To allow for future deconstruction self-lubricating silver-coated bolts were used at all joints. At each mating point bolts were finger-tight first before gradual tightening using spanners in star-shaped patterns. The uniformity of the seal is very important in order to avoid future leaks or cracks. It was advised not to tighten the bolts until the faces of the flanges were flush in order to give room for adjustment during leak detection.

Because atoms are supposed to physically travel down the straight line from the MOT to the science cell, the correct alignment was crucial. First, the *Newport RS series* optical table was adjusted to a perfect horizontal position using level-adjustable stabilizers. Then the vacuum system was meticulously aligned as straight as possible using tools such as a *spirit level* and *self-leveling laser cross-line RIDGIT*.

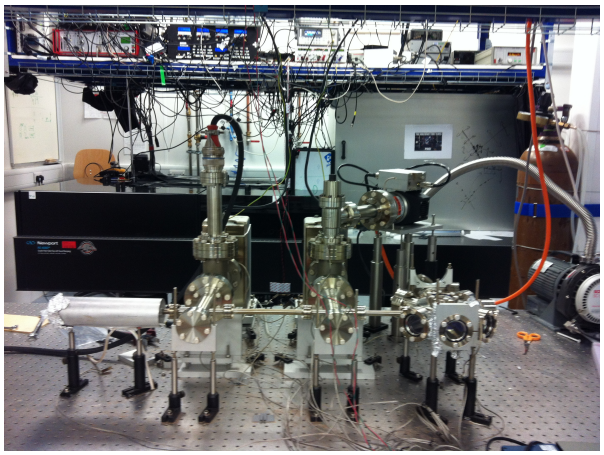

Fig. 2.5 Fully assembled vacuum system

2.4 Baking

It is crucial for an optimal UHV to keep the chambers clean. But cleaning the surface of the walls with a solvent is never enough. This is why every vacuum system requiring a UHV has to undergo baking. Baking is a *"cleaning"* process during which a vacuum system is uniformly heated up and kept at high temperatures for a period of time and slowly cooled down to room temperature. The reason is that most of the contaminants that limit the pressure are absorbed by the walls of vacuum chambers. At UHV pressures these contaminants get desorbed but are not effectively pumped out of the system. During baking the high temperature exponentially accelerates the outgassing of impurities, traces of water and hydrocarbons trapped inside the metal components. These particles are then removed from the system by the pumps. This is why after the cool down the pressures in the systems tend to be orders of magnitude lower than at the start. The pressure and temperature in the system are expected to follow a trend similar to the Clausius-Clapeyron $\ln(P) \propto \frac{1}{T}$.

Before baking, the scroll pump and the turbo pump lowered the pressure inside the system to 10^{-6} mbar. All of the glass parts were covered with aluminum foil for protection. In the case of the science cell we put a metal tube around it to protect the AR coated walls from any damage from direct contact with the heating elements. Then the whole system was wrapped in *Tyco Thermal Controls isopad TeMS2* resistive heating tapes controlled by *Clairtronic 10551* variacs. For monitoring local temperatures we attached thermocouples to the surfaces of the chambers that are controlled by the same variac. This was important in order to decouple different parts of the system during heating and cooling for better control of the temperature. To minimize the loss of heat during baking, the system was wrapped in an insulating layer of fiberglass material followed by several layers of aluminum foil as shown in Figure 2.6. The

ion pumps had heating elements included, so by attaching variacs to them we were able to bake the system in its entirety. After the system was ready to be baked, the voltages across

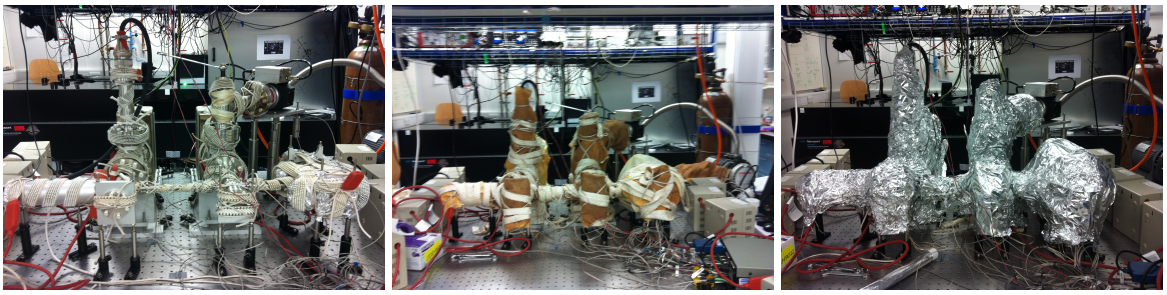

Fig. 2.6 From left to right: 1. The system is wrapped in heating tapes controlled by Variacs. 2. Fiberglass insulation layer. 3. Aluminum foil insulation layer.

heating tapes were gradually increased. It is very important to vary the temperature very slowly, about 2-3 °C/min, and evenly across the system. Any sharp spatial or time gradients of the temperature could cause damage to the system due to differential expansion of materials of the chamber. This is especially important at the glass-metal boundaries of some elements. The temperatures from the thermocouples were acquired using a 16-channel *Stanford Research Systems SR630* monitor and logged using the LabView program connected with *SR630* over a *General Purpose Interface Bus (GPIB)*. During the procedure the voltages from the variacs were manually tuned to insure smooth temperature changes.

With our system we ended up baking two times. The first time we heated the system up to 150 °C, just below the indium melting point. During the first bake we discovered a few leaks, so we decided to cool down the system back to room temperature to close the leaks before baking became irreversible. As mentioned before once the indium seal has melted, the vacuum system cannot be broken apart without loss of the atom sources, due to the danger of exposing them to the air. After a round of leak detection and careful tightening of the flanges we started the second round of baking.

The second time the system was heated up all the way to 210 °C. In theory higher temperatures yield lower pressures after the cool down, but sensitivity of some of the vacuum parts to high temperatures limited the maximum temperature. For example, the ion pumps' permanent magnets begin to lose magnetization above 250 °C, whereas the maximal bakeout temperatures of the Science Cell and viewports are 280-300 °C and 350 °C respectively. It is beneficial to keep the extremities of the system, which are farthest from the powerful pumps, hotter than the middle bulk throughout the baking procedure. It helps to avoid condensation of particles in areas that are less effectively pumped. The pressures during the baking procedure are monitored using gauges of the ion pumps. They tend to be less accurate below 10^{-10}

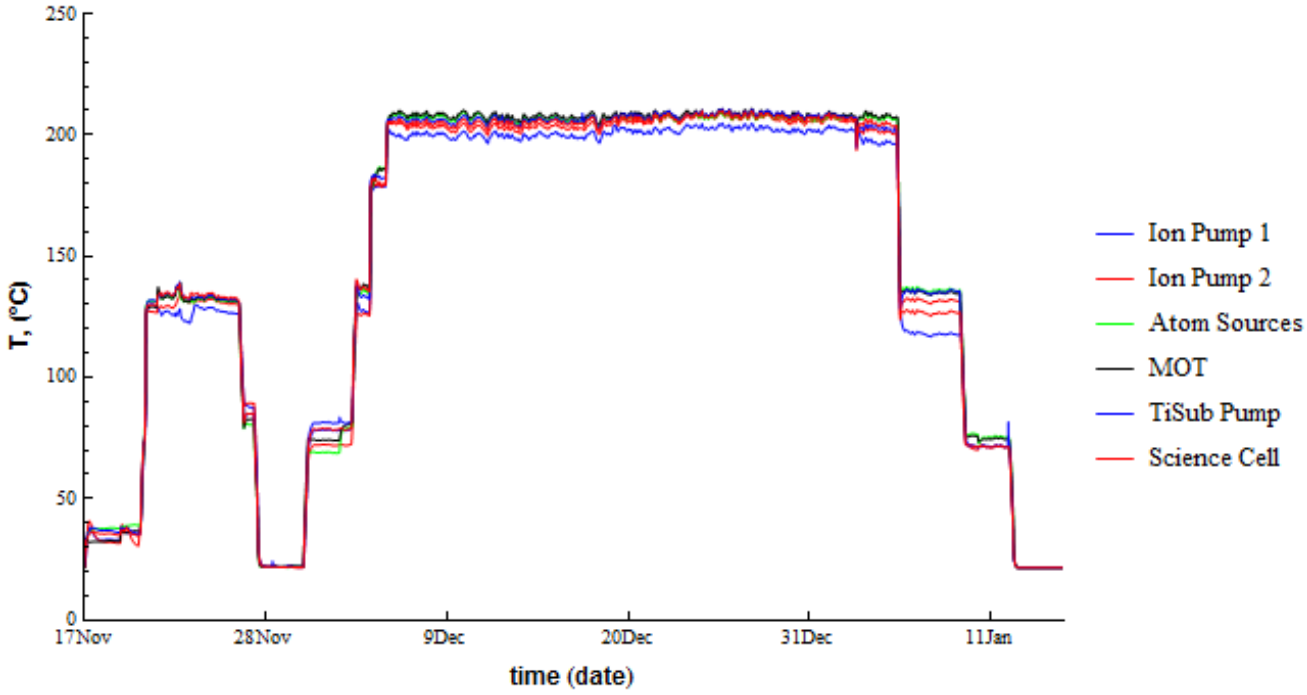

Fig. 2.7 The temperature of the main parts of the system during both baking stages.

mbar, but we found it a sufficient source of information. The temperature and pressure curves against the baking date are shown on Figure 2.7 and 2.8.

During the final cooldown as pressures lowered to 10^{-8} mbar, the turbo and scroll pumps were isolated by sealing off the system using the valve. We started baking at pressures of about 10^{-7} mbar and after the whole procedure we got to 10^{-12} mbar at the science cell side and 10^{-11} at the MOT side. The benefits of baking are clear on the Log plot of Pressure vs $\frac{1}{T}$ that are shown in Figure 2.9. The blue curve represents the first baking round starting heating at point 1 and finishing cooling at 2. The red curve is the second round starting from point 3 and finishing at 4. As was expected the heating and cooling trends are approximately linear. The vertical separations between the start and the finish exemplify the drop in pressure resulting from the baking procedure.

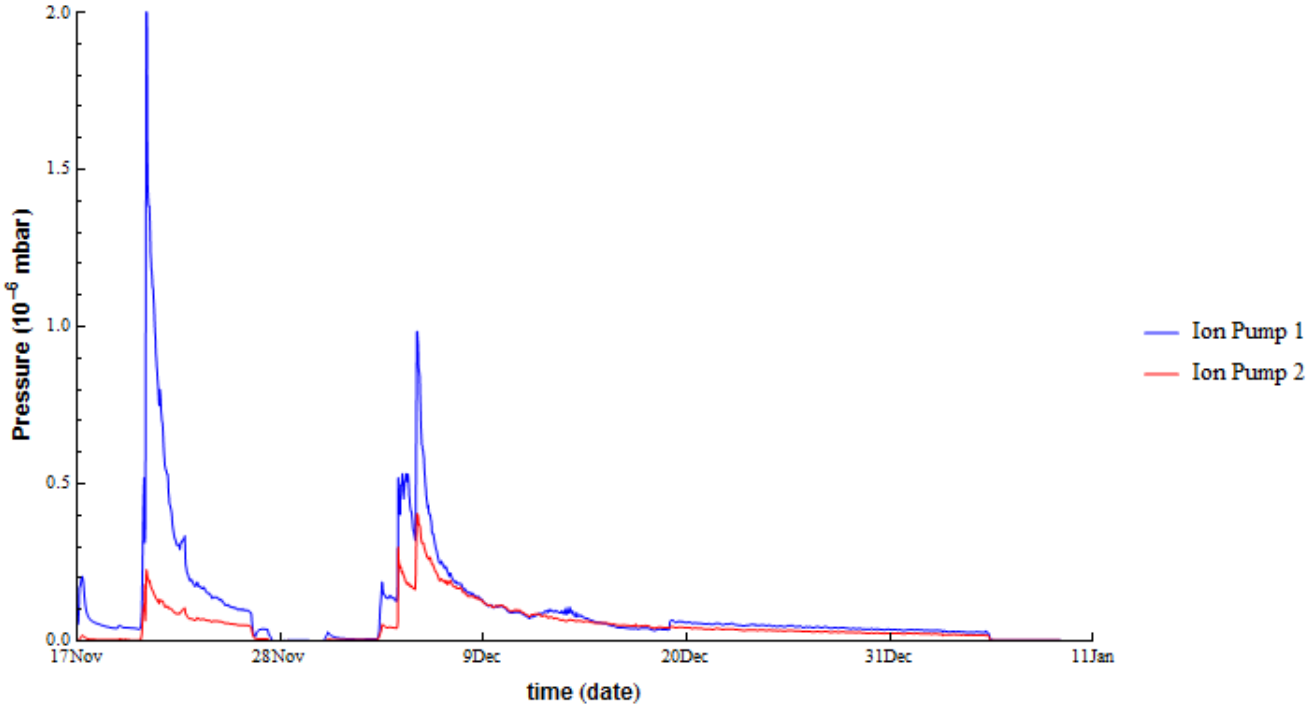

Fig. 2.8 The pressure in the system measured by ion pump 1 and ion pump 2 during both baking stages.

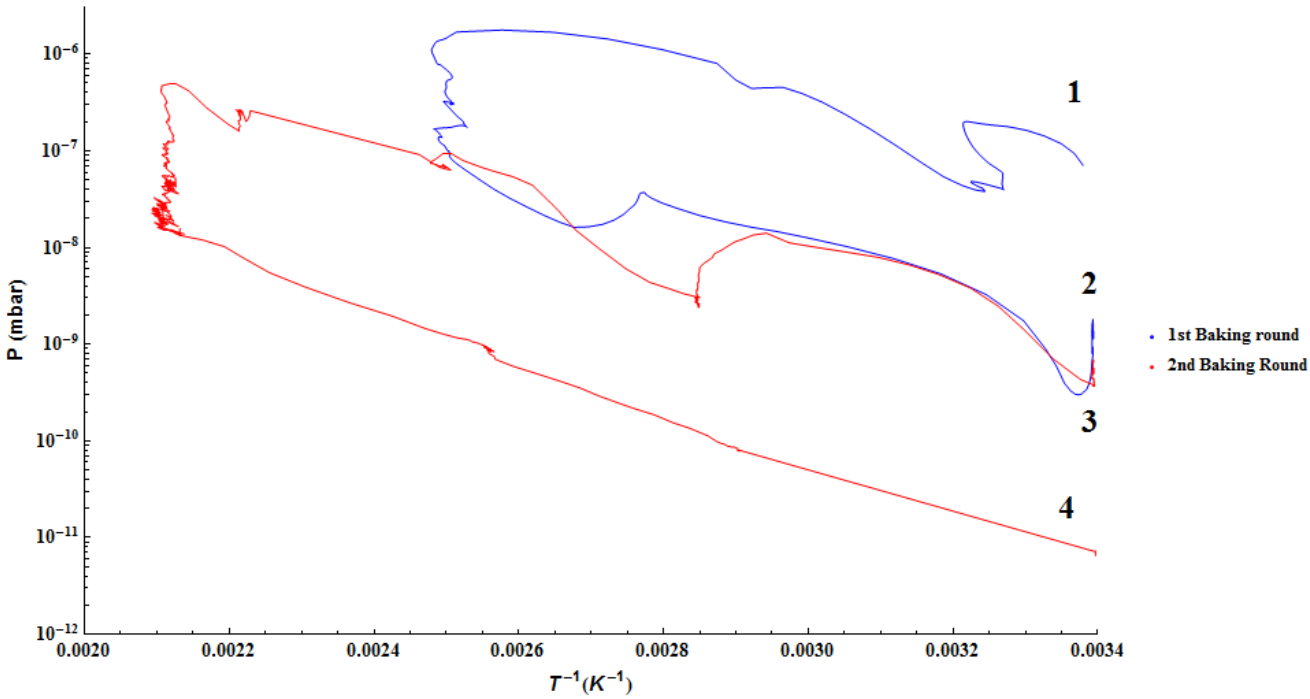

Fig. 2.9 The final Log plot of pressure vs $\frac{1}{T}$ of the bakeout. The blue curve is the first baking round from 10^{-7} mbar (1) to 10^{-9} mbar (2), the red curve is the second baking round from 10^{-9} mbar (3) to 10^{-12} mbar (4).

2.5 Notes on troubleshooting

Every bakeout entails dealing with various problems. Here are the few that we had to face:

- **Power Cuts.** We have had two power cuts that happened over the holidays, when no one was in the lab. It was helpful to have essential electronics, like variacs and Ion pumps, plugged into the uninterruptible power supplies, *UPS*. Since imhomogeneity in the temperature is potentially damaging, the sudden cool down due to the power cut could be ruinous for the vacuum system. These precautions give some extra time for dealing with unexpected issues.

- **Leaks.** The main headache with the vacuum systems is, of course, leaks. Before sealing off the system the method we used for detecting leaks involved helium gas and a mass spectrometer. By spraying helium around potential leak sources and noting spikes in mass spectrometer readings, we were able to identify most of our leaks. For big leaks just spraying helium and monitoring pressure readings of the ion pumps is enough. But as leak sources get smaller and more remote from the ion pumps, the sensors are not efficient enough to pick up any difference. This is why a mass spectrometer is a great tool, it directly measures ratios of He to the background gasses. As any other method it has disadvantages too. Once the amount of helium in the room becomes high the measurements become insensitive and unstable, since traces of He gas keep entering and exiting system through the gaps.

  Every time a leak was found we tightened the flanges around the potential sources. It was effective most of the time. In one case, we found that tightening the bolts was opening more leaks than closing, so to seal the leak we used the *Lesker* leak sealant, which fixed the problem.

- **Ion-pump maintenance.** Since we used ion pumps as the main pressure sensors in our vacuum system, it was important to make sure that the pressure values were accurate within the precision specified by the manufacturer. At some point after baking, for the ion pumps it is the period of heaviest load and contamination, the pressure reading became unstable and unreasonably high. One explanation was the appearance of new leaks, but we couldn't detect any. After a thorough step-by-step investigation we realized that the ion pump pressure measurement was obscured by stray currents between electrodes. These currents are usually a result of either a conducting layer of residue from absorption or so called "wiskers" (sharp edges) accumulated on the electrodes. The problem was eliminated by *"high-potting"* the ion pumps, which means a high

voltage is applied to the electrode for a short period of time, burning off any extraneous conducting material. High-potting is usually included in the ion pump functions.

3

Theory of Laser Cooling

Every cold atoms experiment involves a sophisticated cooling and trapping system necessary for reaching the quantum regime. The techniques used in the process exploit interactions of atoms with electromagnetic fields. Although these are purely quantum mechanical processes, some of the phenomena can be presented in terms of classical and semiclassical concepts in the pursuit of the most elegant theoretical framework. The experimental realization of these techniques only started after the invention of the laser and decades of work on manipulating atoms with high precision. Aside from advancing cold atoms experiments, these methods have been very influential for the fields of atomic spectroscopy and atomic clocks. In this chapter, I will go through brief theoretical descriptions of phenomena crucial to the understanding of our experimental sequence.

3.1 Theory of Laser cooling and trapping

The two forces

There are three processes that constitute all of the atom-light interactions: spontaneous emission, absorption and stimulated emission of photons. The first two of these processes create a scattering force on the atom, while the last two are responsible for the dipole force. These forces are used in various stages of our cooling and trapping system with distinct purposes. Some of the characteristics are noted in Table 3.1.

The electromagnetic wave induces a dipole moment, $\boldsymbol{d} = -e\boldsymbol{r}$, in the atom. The interaction Hamiltonian between this dipole moment and the electric field is:

$$\mathscr{H} = -\boldsymbol{d} \cdot \boldsymbol{E}(\boldsymbol{r}, t) \tag{3.1}$$

	Scattering force	**Dipole force**
Fundamental processes	absorption and spontaneous emission	absorption and stimulated emission
Classical interpretation	absorption and reflection	refraction
Favorable detuning range	$\delta \approx 0$	large δ
Relative strength	weaker (due to saturation)	stronger
Used in:		
Doppler Cooling (Optical molasses)	✓	
Sub-Doppler Cooling (Sisyphus Cooling, Gray Molasses)	✓	✓
Optical Trapping		✓

Table 3.1 Some characteristics of Scattering and Dipole forces

where $\boldsymbol{E}(\boldsymbol{r},t)$ is the electric field operator. Using a model of the two-level atom interacting with a plane wave in three dimensions, it is possible to derive the total force on the atom (3.2):

$$\boldsymbol{F}_{\textbf{total}} = \hbar\boldsymbol{k}\underbrace{\frac{\Gamma}{2}\cdot\frac{I/I_s}{1+I/I_s+(2\delta/\Gamma)^2}}_{\text{Scattering force}} + \underbrace{-\frac{\hbar\delta}{2}\cdot\frac{\nabla(I/I_s)}{1+I/I_s+(2\delta/\Gamma)^2}}_{\text{Dipole force}} \tag{3.2}$$

where $\hbar\boldsymbol{k}$ is the momentum of the photon, Γ is the linewidth of the transition, δ is the detuning of the light from the resonance ($\delta = \omega_{\text{light}} - \omega_{\text{transition}}$), I is the intensity of the light and I_s is the saturation intensity of the transition. A detailed derivation can be found in [39].

The first part is the scattering force, $\boldsymbol{F}_{\text{scatt}}$. It can be expressed in terms of the scattering rate , R_{scatt} and the momentum transferred from the photon to the atom, $\hbar\boldsymbol{k}$. This originates from the fact that the force is equal to the rate of change of momentum of the atom. The second part is the dipole force, $\boldsymbol{F}_{\text{dip}}$. It is proportional to the gradient of the field intensity, which makes it suitable for optical traps. Unlike the scattering force, on resonance $\boldsymbol{F}_{\text{dip}} = 0$. For large detunings, $|\,\delta\,| \gg \Gamma$, the dipole force equals to the derivative of the light shift as a

result of the AC Stark effect [17]

$$\boldsymbol{F}_{\text{dip}} \simeq -\nabla\left(\frac{\hbar\Omega^2}{4\delta}\right) \tag{3.3}$$

where Ω is the Rabi frequency of the transition.

In following sections, I will discuss the particular methods we use to cool and trap ^{39}K atoms in our experimental setup. All of the methods harness to some degree the effects of the forces we discussed above.

3.1.1 Doppler Cooling

This section outlines cooling and trapping methods that rely purely on $\boldsymbol{F}_{\text{scatt}}$. As was discussed previously, light has a mechanical effect on atoms. On a macroscopic scale, the radiation pressure is partially responsible for the direction of a comet's tail, which points away from the radiation. Radiation pressure also compensates for the gravitational pull in stars [17].

Optical Molasses

Optical molasses is a cooling technique that uses momentum transfer between the photons and atoms to reduce the velocity distribution of the atomic cloud. The temperature of a classical gas is determined by the width of the velocity distribution according to the Maxwell-Boltzmann distribution as shown in Figure 3.1. To cool atoms it is necessary to find a way to decrease the entropy of the gas. The scattering force, i.e. spontaneous emission, is the mechanism through which Doppler cooling methods dissipate energy out of the atomic cloud.

During the scattering, the atom undergoes consecutive absorption and spontaneous emission cycles. The absorption of a photon with energy $\hbar\omega$ results in a momentum transfer, $\hbar\mathbf{k}$, to the atom, along with the promotion of the valence electron into the higher energy state. Following spontaneous emission, a photon is released in a random fashion with the electron returning to its ground state. After many cycles, the lost momentum averages out. As a result, the atom feels a net radiation force in the direction of light propagation, proportional to the absorbed momentum per recoil.

$$\boldsymbol{F}_{\text{scatt}} = R_{\text{scatt}} \cdot \hbar\boldsymbol{k} \tag{3.4}$$

This mechanism assumes a two-level atom in resonance with the photon frequency. Atoms in a thermal gas have finite velocities, which lead to a Doppler shift $\delta^{\pm}_{Doppler} = \delta \mp kv$. By using two red-detuned ($\delta < 0$) counter-propagating beams it is possible to slow down

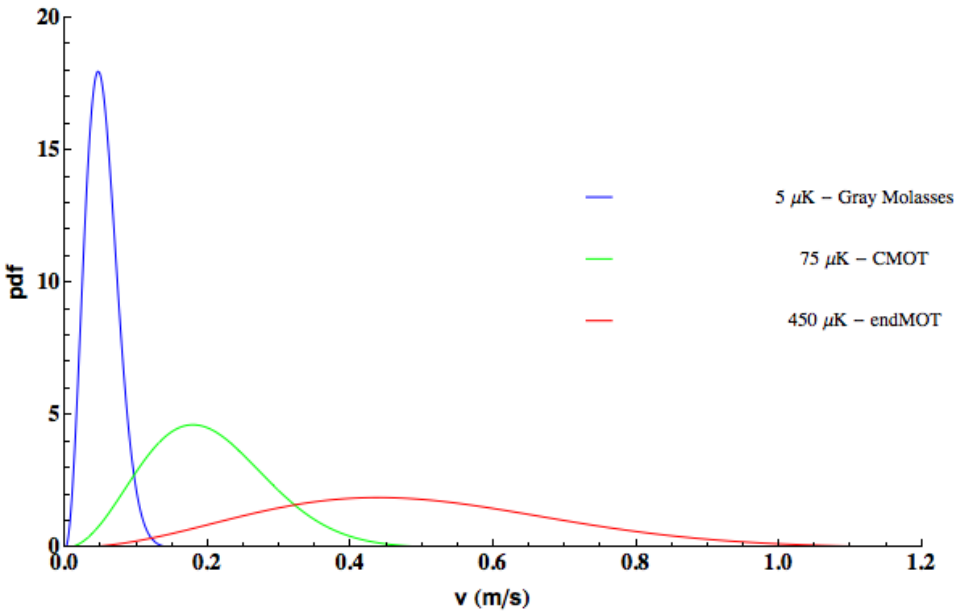

Fig. 3.1 Velocity distributions of atoms in a gas according to the Maxwell-Boltzmann distribution. The three curves of normalized distributions of velocities correspond to the following temperatures: $5\mu K$ - the temperature we achieve after gray molasses cooling technique, $75\mu K$ - after compressed MOT with D1 and D2 light, and $450\mu K$ after the end MOT trap. All of the cooling steps will be discussed in this chapter as well as chapter 4.

atoms moving in both positive and negative directions, since atoms will be absorbing mostly from a beam opposite to its direction of motion. The velocity-dependent detuning is used to target hotter atoms in the cloud to reduce the velocity distribution, which creates a trap in momentum space for the coldest atoms in the cloud. The schematic of this method is shown in Figure 3.2.

In our experiment, we provide a cooling force for atoms along all three dimensions. We use six beams in total around our MOT chamber, where three counter-propagating pairs of laser beams reduce the velocity distribution of atoms in the x, y and z directions. The optical molasses step, as described so far, comes after the atoms are trapped in the Magneto-Optical trap, which itself uses molasses as a confining method for momentum space.

MOT

As atoms cool down in the optical molasses they are free to diffuse out of the intersection area of the beams. It is beneficial to trap them locally before going into further cooling steps. The magneto-optical trap accomplishes this by adding a spatially-dependent detuning, which results in a position-dependent net radiation force.

A weak magnetic field gradient is used to create a position-dependent splitting of the

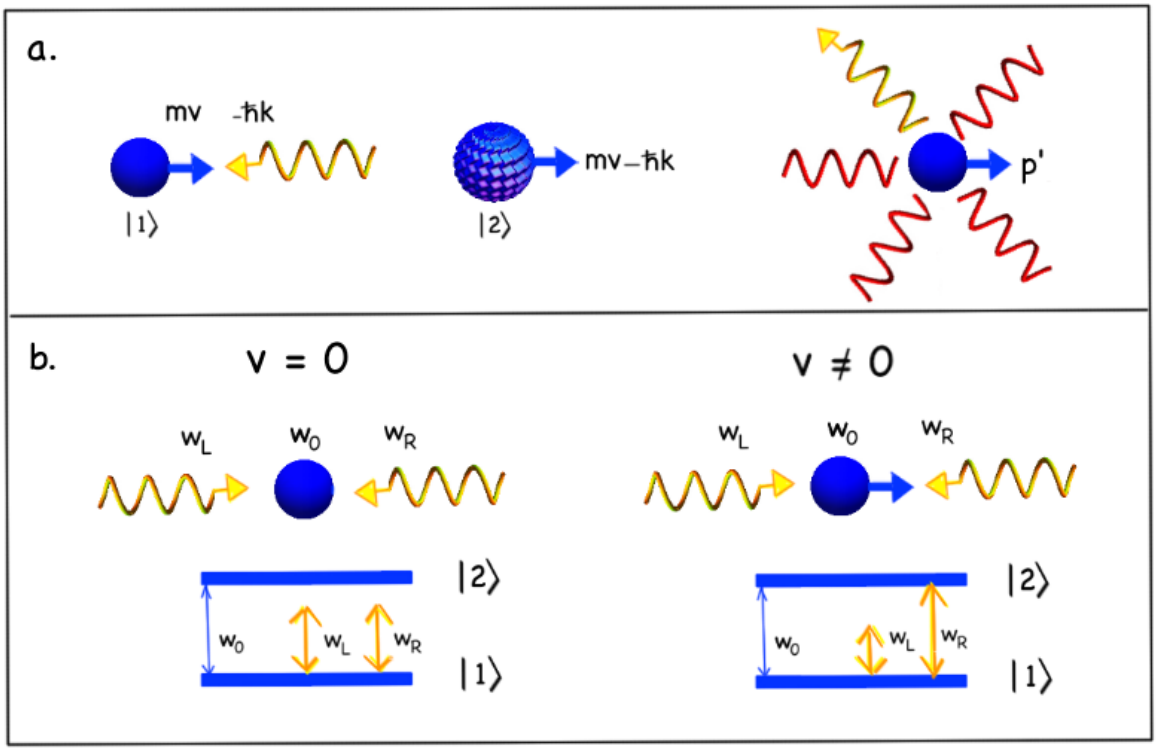

Fig. 3.2 a. A scattering process: photon gets absorbed and emitted in a random fashion while conserving energy and momentum. **b.** Red-detuning the counter-propagating laser beams motivates atoms to absorb photon preferentially from opposing in direction beam.

energy levels by the Zeeman effect [17]:

$$E_{\mathrm{ZE}}(z) = g_{\mathrm{F}}\mu_{\mathrm{B}}m_{\mathrm{F}}B(z) \tag{3.5}$$

where μ_{B} is the Bohr magneton, g_{F} is the Lande g-factor and m_{F} is the z-component of F - the total angular momentum of the atom. By combing this effect with the two counter-propagating beams of opposite circular polarization, we create an imbalance in the radiation force as illustrated in Figure 3.3

In the experimental setup for the MOT we use the same six beams we use for optical molasses, with the addition of a quadrupole magnetic field created by two magnetic coils in an anti-Helmholtz configuration as shown in Figure 3.4. It is very important to coordinate the polarizations of the beams with the direction of magnetic field.

The MOT is a very robust trap with a high capture velocity. This makes it possible for us to load atoms straight from the vapor background at room temperature, after which the magnetic field is turned off to begin the optical molasses stage purely for cooling. The magnetic field that creates spatial confinement in the MOT gets in the way of deeper cooling

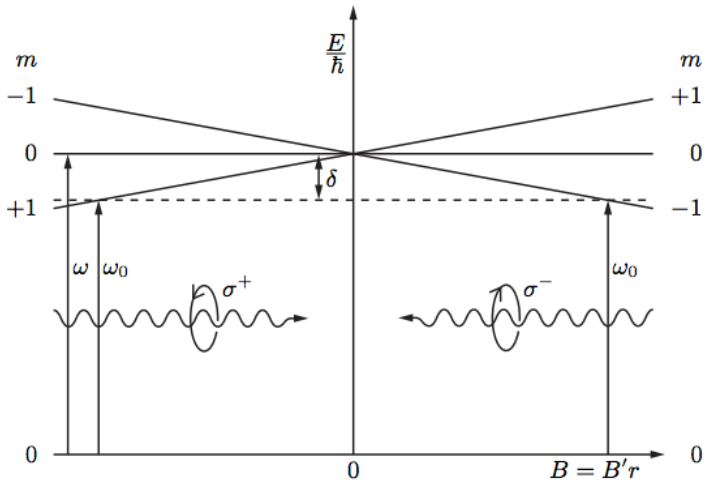

Fig. 3.3 One-dimensional scheme of the MOT mechanism with a single ground state and triplet split excited states. Atoms that move farther away from the center, get closer to the resonance of the light beam in the opposite direction by the Zeeman effect. $\sigma^{\pm}$ only affects $\Delta = \pm 1$ transitions. Figure from [7]

effects of optical molasses that I will discuss in the coming sections.

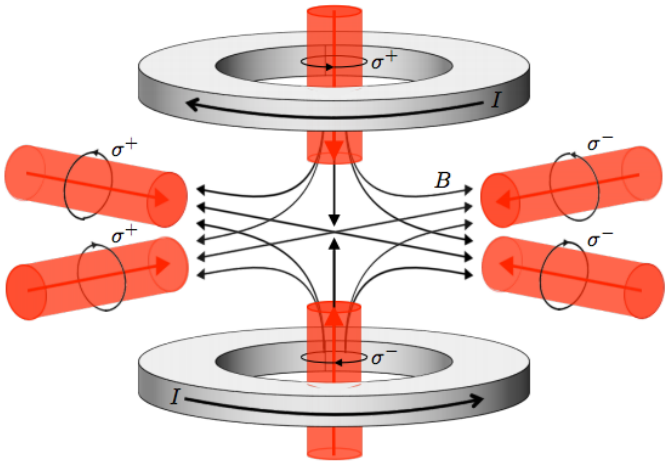

Fig. 3.4 3D MOT used in our experiment. Six red-detuned beams of opposite polarizations are combined with quadrupole field created by two coils in the anti-Helmholtz configuration. Figure from [7]

Doppler Limit

The scattering force by itself can only cool atoms to a fixed limit. This limit is a point where Doppler cooling is balanced by the heating resulting from the discrete recoil events of absorption and spontaneous emission. This gives the Doppler temperature

$$T_{\mathrm{D}} = \frac{\hbar\Gamma}{2k_{\mathrm{B}}} \tag{3.6}$$

For ^{39}K, the Doppler temperature is 146μK, which corresponds to velocity of 12 cm/s. As mentioned in the introduction, for potassium, due to its poorly resolved hyperfine structure, T_D is not an easy barrier to overcome in terms of cooling.

3.1.2 Theory of Sub-Doppler Cooling

The scattering force by itself can only be used for Doppler cooling. But in combination with the dipole force and the multiple energy levels that real atoms possess, it is possible to reach temperatures below the Doppler limit using more sophisticated methods.

Sisyphus Cooling

The temperatures below the Doppler limit can be achieved in optical molasses via a mechanism known as Sisyphus cooling. It requires magnetic sub-levels of the ground state

like an m_J structure of the $J = 1/2$ state of ^{39}K (Figure 4.1). Figure 3.5 shows a schematic description of the process for a system consisting of a $J = 1/2$ ground state and a $J' = 3/2$ excited state.

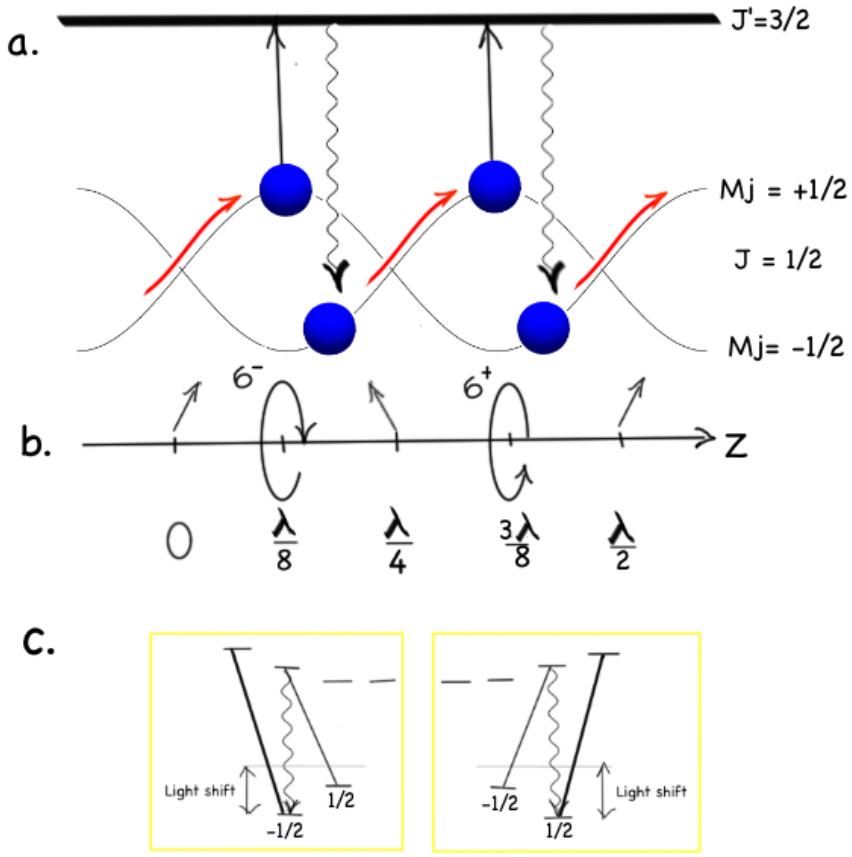

Fig. 3.5 a. A schematic of Sisyphus cooling in one dimension. The periodic energy splitting of $m_J = +1/2$ and $m_J = -1/2$ makes atoms loose kinetic energy as they move from the lowest point of the potential to the highest. There, via absorption and spontaneous emission, atoms are bumped down to a lower energy state. **b.** A length scale in terms of λ of the optical molasses beams, along with the respective polarization variation along the z axis. **c.** The energies of the states at the position of σ^+ and σ^- polarizations. Absorption of the circularly-polarized light followed by spontaneous emission transfers the population into the state with lowest energy/largest light shift.

For large detunings, dipole force effects come into play and we can't approximate σ^+ and σ^- counter-propagating beams as independent anymore. The two beams interfere creating a standing wave with a periodic polarization gradient along the axis, which causes a spatially-periodic modulation of the energies of the magnetic sub-levels due to the AC Stark effect (see Figure 3.5c). If an atom in a $m_J = -1/2$ state at the bottom of the hill at $\lambda/8$ climbs the hill up to $3\lambda/8$ it loses kinetic energy. In addition it increases its probability to transition

into the $m_J = 1/2$ state through $J' = 3/2$. At that point with energy loss $E_{\text{light shift}}$, the atom is ready to climb a new hill. As atoms go downhill, they gain kinetic energy but due to low chance of being pumped up they lose this energy right away in the next cycle. This way atoms perpetually lose energy as they climb the hills of the optical potential, in the same way as the king Sisyphus in Greek mythology was compelled to role a boulder up the hill only to watch it roll back down time after time.

The limit of this cooling method is reached when atom's energy loss from jumping into the potential minimum is equal to the recoil energy it acquires during the spontaneous emission. The recoil temperature can be found by equating the depth of the potential to the kinetic energy acquired from the recoil:

$$T_{\text{rec}} = \frac{(\hbar k)^2}{2mk_{\text{B}}} \tag{3.7}$$

The recoil temperature and velocity of ^{39}K are 415 nK and 1.34 cm/s respectively. In case of ^{39}K, the limit of sub-Doppler cooling with the optical molasses is much higher due to complex structure of the excited state. Poor resolution of the hyperfine structure of the excited state makes the optical pumping in Sisyphus cooling non-trivial, which results in much higher temperatures, about 34 μK [20]. In our old ^{39}K machine the sub-Doppler step comes after precooling in Doppler optical molasses by increasing the detuning and decreasing the intensity of the light. The final temperatures were about 200 μK [7]. In the new machine, we employ a more effective sub-Doppler cooling technique called gray molasses, which is a sub-recoil technique and can reach much lower final temperatures.

Gray Molasses

The gray molasses technique combines velocity-selective coherent-population transfer (VSCPT) and Sisyphus cooling to achieve temperatures below the recoil limit. Overall, this method results in trapping of the slowest/coldest atoms of the cloud in the so called *dark state*, while hotter ones undergo Sisyphus cooling in the *bright state* until they are cold enough to be transferred into the *dark state*. I will describe some fundamental principles behind this method on the D1 line of ^{39}K below.

Raman Transition and the dark state

In multi-level systems, coherent superpositions between different states may lead to changes in light absorption and propagation. In the Sisyphus cooling mechanism, we already saw how

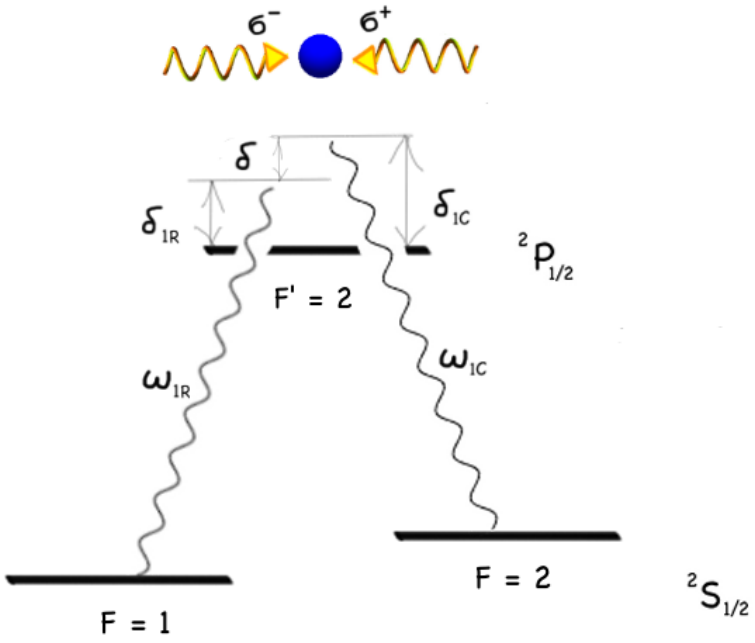

Fig. 3.6 A three level Λ-system of two ground states $F = 1$ and $F = 2$ of $^2S_{1/2}$ and the excited state $F' = 2$ of the $^2P_{1/2}$ of ^{39}K atom. The Cooling beam of frequency ω_{1C} and detuning δ_{1C} couples the $F = 2 \rightarrow F' = 2$ transition, whereas the Repump beam, of ω_{1R} and δ_{1R}, couples the $F = 1 \rightarrow F' = 2$ transition

a departure from the simple two-level system we discussed in Doppler cooling to a three level system brings out complex phenomena beneficial to cooling atoms. Here we will go over the effects of coherent superpositions in a three level system which is fundamental to the gray molasses mechanism. The derivation related to the Raman transition follows the description in the lecture notes by K. Marzlin [27].

A simple Λ-system with two ground states $|F = 1\rangle$ and $|F = 2\rangle$, and an excited state $|F' = 2\rangle$ of the D1 line of ^{39}K is shown in Figure 3.6. For consistency we will use the same nomenclature for beam frequencies and detunings as in the experimental section. The coupling for the $|F = 1\rangle$ to $|F' = 2\rangle$ is made through a repump beam of frequency ω_{1R} and detuning δ_{1R}, whereas the transition $|F = 2\rangle$ to $|F' = 2\rangle$ corresponds to a cooling beam of frequency

ω_{1C} and detuning δ_{1C}. The Hamiltonian of this system in the rotating wave approximation is

$$\begin{aligned} H &= \begin{pmatrix} E_{2'} & \hbar\Omega_1 e^{-i\omega_{1R}t} & \hbar\Omega_2 e^{-i\omega_{1C}t} \\ \hbar\Omega_1^* e^{i\omega_{1R}t} & E_1 & 0 \\ \hbar\Omega_2^* e^{i\omega_{1C}t} & 0 & E_2 \end{pmatrix} \\ &= E_{2'}\mathbb{1}_{3\times 3} + \begin{pmatrix} 0 & \hbar\Omega_1 e^{-i\omega_{1R}t} & \hbar\Omega_2 e^{-i\omega_{1C}t} \\ \hbar\Omega_1^* e^{i\omega_{1R}t} & E_1 - E_{2'} & 0 \\ \hbar\Omega_2^* e^{i\omega_{1C}t} & 0 & E_2 - E_{2'} \end{pmatrix} \end{aligned} \tag{3.8}$$

where $E_{2'}$, E_1 and E_2 are the energies of the excited and ground states, and Ω_1 and Ω_2 are the corresponding Rabi frequencies of the transitions. By applying a unitary transformation $\widetilde{\psi}_{1,2} = e^{-\omega_{1,2}t}\psi_{1,2}$ it is possible to remove the time dependance. The time-independent Hamiltonian is

$$H = E_{2'}\mathbb{1}_{3\times 3} + \hbar \begin{pmatrix} 0 & \Omega_1 & \Omega_2 \\ \Omega_1^* & \delta_{1R} & 0 \\ \Omega_2^* & 0 & \delta_{1C} \end{pmatrix} \tag{3.9}$$

where $\delta_{1R/1C} = \omega_{1R/1C} - \frac{E_{2'}-E_1}{\hbar}$ are the detuning of the repump and cooling beams. For a two photon resonance, $\delta_{1R} = \delta_{1C} = \Delta$, it is easy to show that there is such an eigenstate

$$|\psi_D\rangle = \frac{\Omega_2}{\Omega}|F=1\rangle - \frac{\Omega_1}{\Omega}|F=2\rangle \tag{3.10}$$

that does not interact with light. Here, $\Omega = \sqrt{\Omega_1^2 + \Omega_2^2}$. To double check, the action of the Hamiltonian on the dark state is given by

$$H|\psi_D\rangle = \hbar \begin{pmatrix} 0 & \Omega_1 & \Omega_2 \\ \Omega_1^* & \delta_{1R} & 0 \\ \Omega_2^* & 0 & \delta_{1C} \end{pmatrix} \begin{pmatrix} 0 \\ \frac{\Omega_2}{\Omega} \\ -\frac{\Omega_1}{\Omega} \end{pmatrix} = \hbar \begin{pmatrix} \frac{\Omega_1\Omega_2}{\Omega} - \frac{\Omega_2\Omega_1}{\Omega} \\ \delta_{1R}\frac{\Omega_2}{\Omega} \\ -\delta_{1C}\frac{\Omega_1}{\Omega} \end{pmatrix} = \hbar\Delta \begin{pmatrix} 0 \\ \frac{\Omega_2}{\Omega} \\ -\frac{\Omega_1}{\Omega} \end{pmatrix} \tag{3.11}$$

so the dark state is an eigenstate of the system. This means once atom is in it it does not absorb or emit light any more. Physically, this is a consequence of destructive interference between paths from the ground state to the excited state. As a result of the Raman transition it is possible to trap atoms coherently in the dark state without interaction with the cooling and repump beams. This technique is widely used for confining atoms in optical lattices and traps, since the dark states considerably reduce mutual atom interactions through spontaneous emission and absorption of photons [24].

For any set of Rabi frequencies, there is a bright state

$$|\psi_B\rangle = \frac{\Omega_1^*}{\Omega}|F=1\rangle + \frac{\Omega_2^*}{\Omega}|F=2\rangle \tag{3.12}$$

which is orthogonal to $|\psi_D\rangle$ and is coupled to the excited state. For the gray molasses mechanism it is easier to think about the Λ-system of two ground states: $|\psi_D\rangle$ and $|\psi_B\rangle$, and the excited state $|F'=2\rangle$ as shown in Figure 3.7. Spontaneous emission from the excited state can put the atom in either of the $|\psi_D\rangle$ and $|\psi_B\rangle$ states since the dark state is only dark for the two laser modes ω_{1C} and ω_{1R}.

Velocity-selective coherent-population trapping

If the Doppler shift of atoms is included in the derivation of the dark and bright states, then the two photon resonance needs to be corrected $\delta_{1R} - \delta_{1C} = \delta_{\text{Doppler}}$. This way it is possible to create a dark state that is velocity-selective for atoms [3]. In cooling methods solely based on VSCPT, the small detunings are usually used to trap the coldest ($v \approx 0$) atoms in the cloud. The dark state is populated by the spontaneous decay. Since the last recoil due to spontaneous emission participates in the redistribution of the velocities and cooling, this method is not constrained to the one-photon recoil temperature limit. The time the atom stays in the dark state is $\propto 1/v$. So the colder the atoms, the longer they stay in the dark. However, due to the random character of spontaneous emission, there is nothing stopping other atoms from diffusing towards higher velocities. These atoms never get colder, so at the end, not all of the atoms participate in the cooling mechanism and get trapped [43]. It was obvious that to take full advantage of this cooling method there needs to be a friction force added to the mechanism to confine the atoms in momentum space.

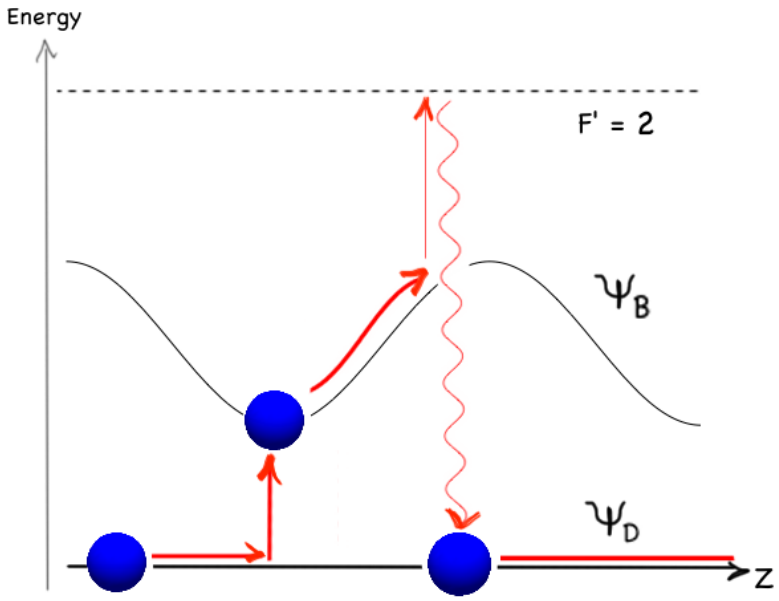

Fig. 3.7 Gray molasses scheme in one direction in the transformed basis. For positive detunings, Δ, the ground states $F = 1$ and $F = 2$ interfere and split into a dark $|\psi_D\rangle$ and a bright $|\psi_B\rangle$states. In the presence of a polarization gradient, the energy of the bright state is spatially modulated. By moving along the z axis, atoms loose kinetic energy while climbing the potential hill, similar to Sisyphus cooling. The atoms with lowered velocity get captured by a dark state through spontaneous emission. The motional coupling between the dark and the bright states happens mostly at the potential minima.

Combined cooling mechanism

This force again comes from dipole interaction and Sisyphus cooling. The derivation of the dark state relied on equal detunings of the repump and cooling beams from the excited state. However, the value of this detuning, Δ was not relevant. Now, for $\Delta > \Gamma$ the dipole force can create a Sisyphus effect on the atom for a bright state $|\psi_B\rangle$ and an excited state $|F' = 2\rangle$ as shown in Figure 3.7. As was mentioned before, the gray molasses mechanism is clearer in a transformed basis where the ground states are $|\psi_B\rangle$ and $|\psi_D\rangle$, and the excited state remains $|F' = 2\rangle$. The dark state does not get affected by the AC Stark shift, since it doesn't interact with light. As a result the potential of the dark state is flat. On the other hand, the bright state potential, for large detunings from the resonance, becomes periodic in a similar way as was described for Sisyphus cooling.

Since now the mechanism involves Sisyphus cooling on the side, it is possible to work in the two-photon resonance regime, $\delta = 0$. Now, only the coldest atoms get trapped in the dark state. Others undergo a loss of kinetic energy in the perpetual cycles of climbing the hills of the bright state potential. As atoms cool down in the polarization gradient the probability of jumping into the dark state increases. So eventually, the cooled atoms transition to the dark

trap to join other cold atoms. In the experimental setting, the main two connections between the dark and the bright state come from dipolar coupling via off-resonant excited hyperfine states, such as $|F' = 2\rangle$, and motional coupling due to any spatial variations of the dark state internal wave function induced by polarization or intensity gradients [31].

We use the gray molasses technique as a final cooling step before atoms are optically pumped and loaded into the magnetic trap to be transferred into the science cell. Since the capture velocity of the gray molasses is quite low it is advisable to pre-cool atoms beforehand. After initial trapping in the MOT, atoms are cooled and compressed by a compressed MOT technique, which also uses the gray molasses method as its basis. As will be shown in the next Chapter, both CMOT and gray molasses turn out to be robust cooling techniques in terms of both final temperature and number of atoms.

4

Laser Cooling Experiment

In this chapter, I will describe the experimental realization of the laser cooling and trapping discussed in the previous chapter. The first part of the chapter will cover the experimental setup. The second part will go over results of the Doppler and sub-Doppler cooling sequences.

4.1 Experimental Setup

Cooling and trapping ^{39}K

The methods described in the previous chapter need to be carefully tailored for the atoms used in the experiment. Usually, simple two- or three-level atom approximations are not representative of real atomic structure. In our case, ^{39}K has a rich hyperfine structure as shown in Figure 4.1. The $|F = 2\rangle \rightarrow |F' = 3\rangle$ transition of the D2 line is used for the main Doppler cooling beam as the closest candidate for a closed transition. The selection rule $\Delta F = 0, \pm 1$ ensures that absorption and spontaneous emission processes cycle in between $|F = 2\rangle$ and $|F' = 3\rangle$. However, the closeness of the hyperfine levels of $^2P_{3/2}$ sometimes results in atoms being transferred from $|F = 2\rangle \rightarrow |F' = 2\rangle$. From here atoms can decay down to the $|F = 1\rangle$ state. To compensate for this we use a repump beam that pumps atoms from $|F = 1\rangle \rightarrow |F' = 2\rangle$, from where they can decay back to the $|F = 2\rangle$ state. For the optimal cooling using the poorly resolved hyperfine structure of the $^2P_{3/2}$ states, both repump and cooling beams have similar intensities and are both red-detuned from the entire excited state manifold.

For the gray molasses mechanism we use the D1 line, $^2S_{1/2}$ to $^2P_{1/2}$. The Λ-system is constructed by a cooling beam of frequency ω_{1C} and detuning δ_{1C}, which couples the $F = 2 \rightarrow F' = 2$ transition, and the repump beam of frequency ω_{1R} and detuning δ_{1R}, which couples the

$F = 1 \rightarrow F' = 2$ transition. Both beams are blue-detuned for the optimal cooling result.

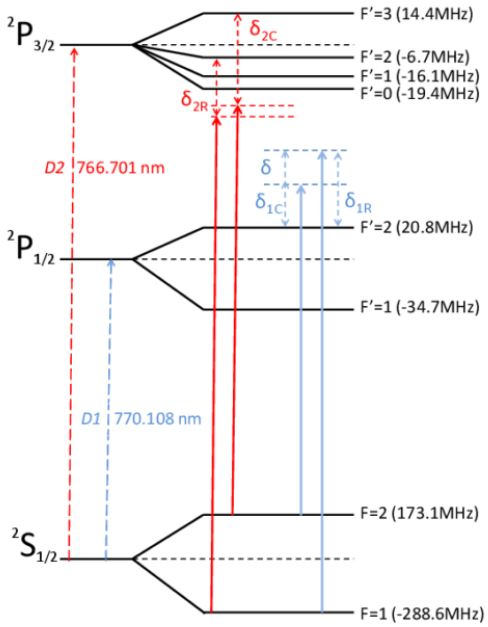

Fig. 4.1 ^{39}K hyperfine structure. We use both D1 and D2 lines for the cooling and trapping sequence. The D2 line is used for Doppler cooling and the D1 is used for Sub-Doppler techniques, e.g. gray molasses. Figure from [34]

Laser setup

All of the processes involving atom-light interactions require light of very narrow linewidths for addressing particular atomic transitions. We use commercial diode lasers of linewidths on the order of 1 MHz, which is below the Doppler width, Hyperfine splitting and natural linewidths of ^{39}K transitions. Natural linewidths of the D1 and D2 lines are $6.03(1)$ MHz and $6.035(11)$ MHz respectively [41].

In spite of the enhanced stability of commercial lasers, continuous locking of the laser to a particular point is required for a stable frequency outcome. Lasers are quite prone to frequency shifting over time due to any external perturbations, including noise and temperature variations. The locking is performed using conventional saturated-absorption spectroscopy of ^{39}K atoms in the vapor cells. The D1 and D2 crossover spectral lines are shown in Figure 4.2. The derivatives of these line shapes are used to perform top-of-fringe laser locking using *Toptica Digilock* for the D2 Laser and *Sacher LB2001* and *SR830* for the D1 Laser.

The overview of the ^{39}K Laser system is shown in Figure 4.3. We use a *Sacher Lasertech-*

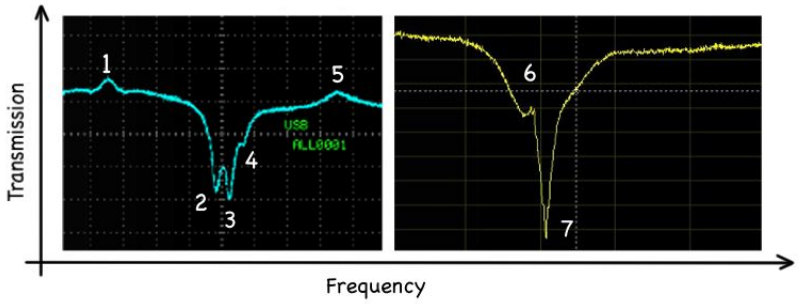

Fig. 4.2 Saturated absorption spectra of D1 line (on the left) and D2 line (on the right) from the oscilloscope. Here D1 line has five features: 1 - is the $|F = 2\rangle \rightarrow |F'\rangle$ transition, 2, 3, 4 - are crossover peaks (we lock our laser to 2), 5 is the $|F = 1\rangle \rightarrow |F'\rangle$ transition. D2 line shows two features: 6 - is $|F = 2\rangle \rightarrow |F'\rangle$, and 7 - is the crossover we lock our D2 laser to.

nik TEC500 laser of 770 nm for the D1 line and a Toptica laser of 767 nm for D2 line. Each laser beam is split in two and passed through a double-pass AOM, which shifts the frequency and alters the amplitude of the repump and cooling beams accordingly. All four beams are then combined using a polarizing beamsplitter cube (PBS) and amplified in the TA up to a total power of 1 W. The power ratios between the beams are controlled using wave plates. After combination, part of the light is split off and used for imaging through careful coupling into a polarization-maintaining (PM) single-mode fiber. The combined light of the D1 and D2 beams is coupled in to a *Shafter+ Kirchhoff GmbH* fiberport cluster 2-to-6 in order to be divided into six beams for the MOT chamber setup.

The laser system was setup with the help of undergraduate students: Sarah Thomas [40] and Yago del Valle-Inclan Redondo [11].

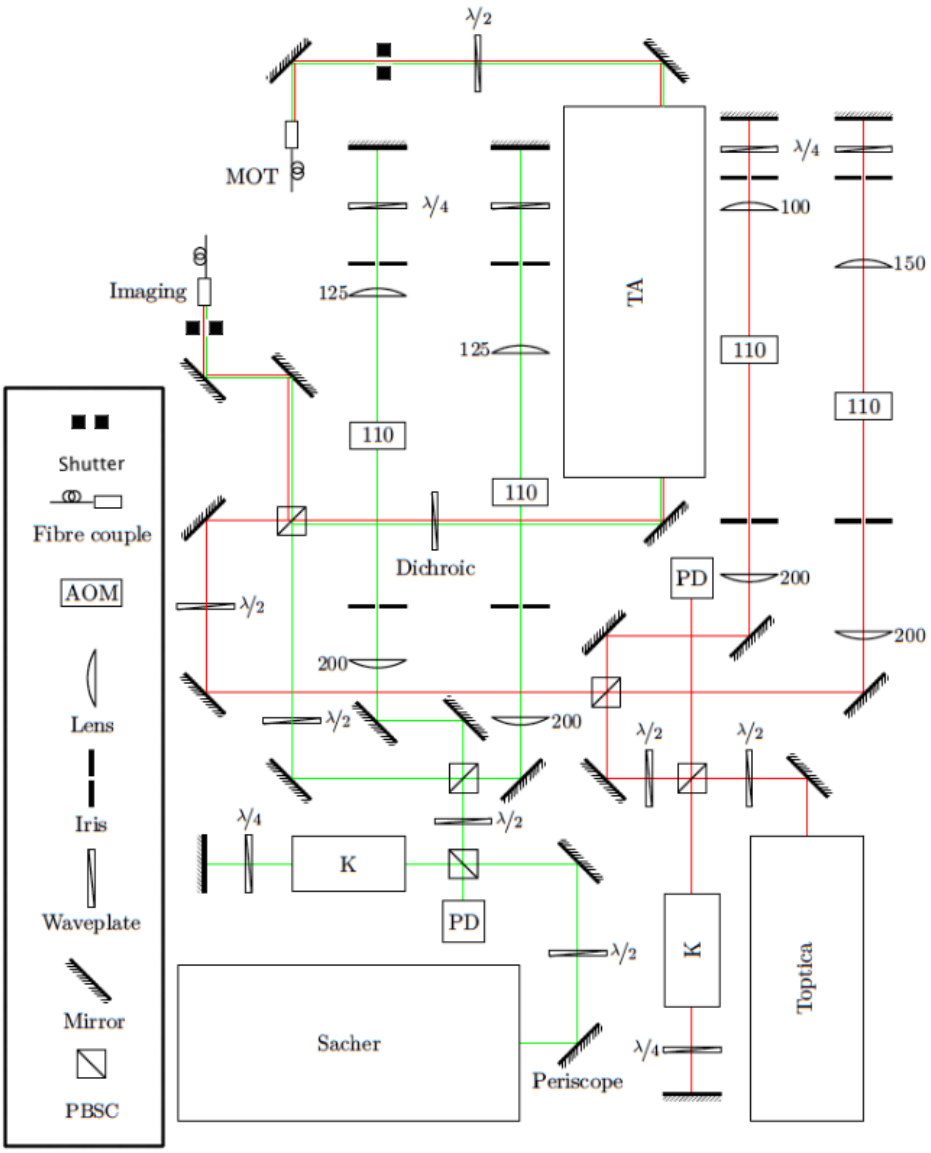

Fig. 4.3 The two-laser optical setup (the diagram is modified from [11]). A Sacher laser is used for the D1 light (green) and a Toptica laser for the D2 line (red). Each laser is locked using saturated absorption spectroscopy using potassium vapor cells. Two AOMs per laser are used to vary the cooling and repump beams accordingly. All fours beams are combined and amplified in the TA. The values on the lenses correspond to the focal length, whereas the numbers on the AOMs correspond to their central frequencies.

Setup of the MOT

The atoms are trapped and cooled for the first time in the MOT chamber. The light beams of the MOT come from the fiber port cluster through polarization-maintaining fibers. Each fiber output passes through a cage system containing a collimation lens and a quarter wave-plate, creating a 3cm diameter circularly polarized beam. Two adjustable mirrors for each beam are used to align the MOT beams. The setup comprises of six beams in total: two counter-propagating pairs in the horizontal plane and one in the vertical plane as was described in the previous chapter (see Figure 3.4).

The magnetic field component of the MOT setup consists of two quadrupole and six compensation coils. The quadrupole coils, in anti-Helmholtz configuration, are used for the MOT trap, confinement of atoms during transport, and will be used for the initial evaporative cooling stage in the science cell. Because of their multi-purpose nature, the coils are mounted on an aluminum translation stage which moves from the MOT to the Science Cell. The current to the coils is provided by a *Delta Electronika, SM 30-200* DC power supply, and controlled remotely using high voltage *SEMIKRON, SEMiX 402GB066HD* IGBT. Due to the high current, the quadrupole coils tend to heat up, which is why we run water through the hollow tubing throughout the experiment. The compensation coils provide three degrees of freedom (x, y, z) to tune the magnetic field in order to cancel the background fields, which are detrimental to the sub-Doppler cooling operation. The details of the coils are compiled in Table B.2 of Appendix B.

Control of the system

Before proceeding to the results of the cooling and trapping sequence, it is worth mentioning the control system we use for communicating with the devices involved in the sequence. Many parameters of the sequence need to be accessed remotely in real time with temporal resolution sometimes reaching tens of μs. This requires a specialized electronic interface. At the software end we use the Cicero Word Generator control package, specifically designed for cold atoms experiments and made available to the public under the GNU General Public License. On the hardware side, the signal from the PC passes down to *National Instruments PXI*-based I/O devices. The PXI chassis creates the analog and digital signals, which are interfaced with the rest of the experiment through optical and capacitive isolation circuits. The isolation helps to avoid damage to the NI Hardware from voltage spikes and other noise in the system [39]. The signal flow of the control system is shown in Figure 4.4.

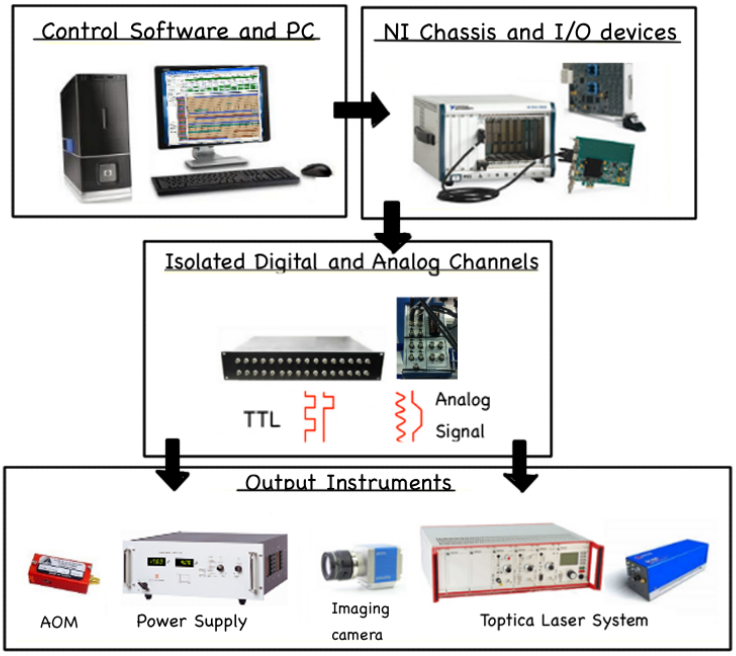

Fig. 4.4 Diagram of the Signal flow in the system. The input sequence from the control software on the PC passes down to the National Instruments PXI-based I/O devices, which generate digital and analog signals. The signals pass through buffer isolated from the NI hardware for the safety of the device. From here, analog and TTL signals proceed as the input of the instruments involved in the sequence.

4.2 Results

Currently, the experimental sequence consists of the following steps: the MOT, closer to the resonance endMOT, compressed MOT using D1 and D2 lines (CMOT), sub-Doppler technique gray molasses, Optical Pumping and magnetic trap. The optical pumping and magnetic trap steps will be covered in the next chapter. All of the optimized parameters needed for this sequence are summarized in Table 4.1. The optimization was done, mainly, by two criteria: to maximize the number of atoms and to minimize the temperature. The temperature of the cloud is acquired using simple time of flight measurements. The number of atoms is calculated from gaussian fits of the atom distributions. Both of these methods are done using fluorescent imaging of the cloud using resonant cooling and repump beams of the D2 line and a *Pco Pixelfly* digital camera. The details of the measurement sequence are described in Appendix A. Here, I will outline the results of the Doppler and sub-Doppler cooling.

MOT

During the operation of the experiment, the pressure inside the Vacuum system is $\sim 10^{-10}$mbar on the side of the MOT chamber, as measured by Ion Pump 1. The atom sources are fired once a day by turning the current of $\sim$ 6A for 1.5min. For the MOT step, the detunings of the cooling and repump beams are -6.2Γ and -2.0Γ respectively. The Magnetic field gradient is $\sim$ 4.5G/cm.

The loading curve of the MOT, which is the number of atoms trapped as a function of time, is shown in Figure 4.5. A rough approximation of the lifetime of the trap was achieved by assuming that the rate of loading of the MOT, $\dot{N}$, is proportional to some constant loading coefficient minus the rate of exponential decay of the trap. From the fit function $N = N_0(1 - e^{-\frac{t}{\tau}})$ the lifetime of the MOT, τ, was measured to be 3.8s. The loading curve also affected the choice of the duration of the MOT step, which was optimized to be about 20 s. It is worth noting that the τ of the MOT varies significantly with the duration of time the atom sources are on during firing. The longer we fire the sources, the more atoms we trap, however it lowers the lifetime of the MOT, which could result in instability of the atom number and short lifetimes in the magnetic trap after the cooling sequence. The optimal time will depend on the subsequent experimental steps, which are currently works in progress.

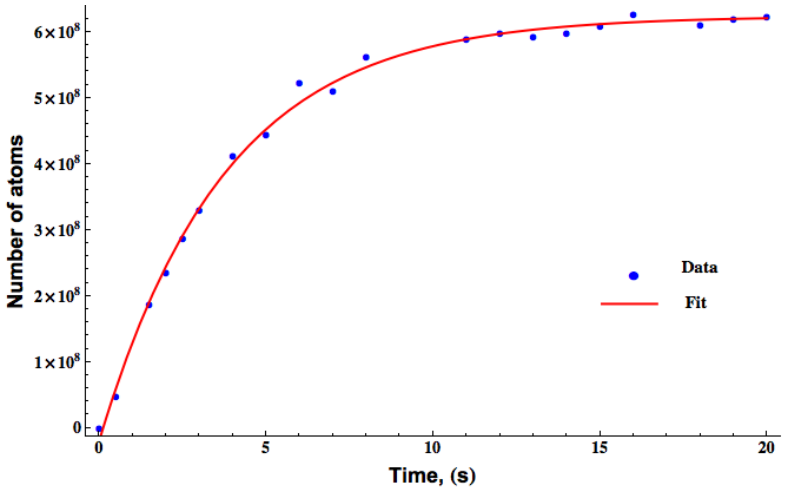

Fig. 4.5 The Number of atoms trapped in the Magneto Optical Trap as a function of time. The fit is given by $N = N_0(1 - e^{-\frac{t}{\tau}})$, where the lifetime of the MOT is $\tau = 3.8$s

Figure 4.6 shows the temperature and atom number measurements of the cloud right after the MOT step. The trap contains up to $(5.8 \pm 0.6) \times 10^8$ atoms at a temperature of about 10 ± 2 mK with a phase-space density[1] of $(4 \pm 1) \times 10^{-12}$. The cloud doesn't have an exact gaussian

[1] The phase-space density is calculated using the peak density of the cloud.

shape, but these parameters produce the highest number of atoms and lowest temperature as a single step as well as a part of the cooling sequence.

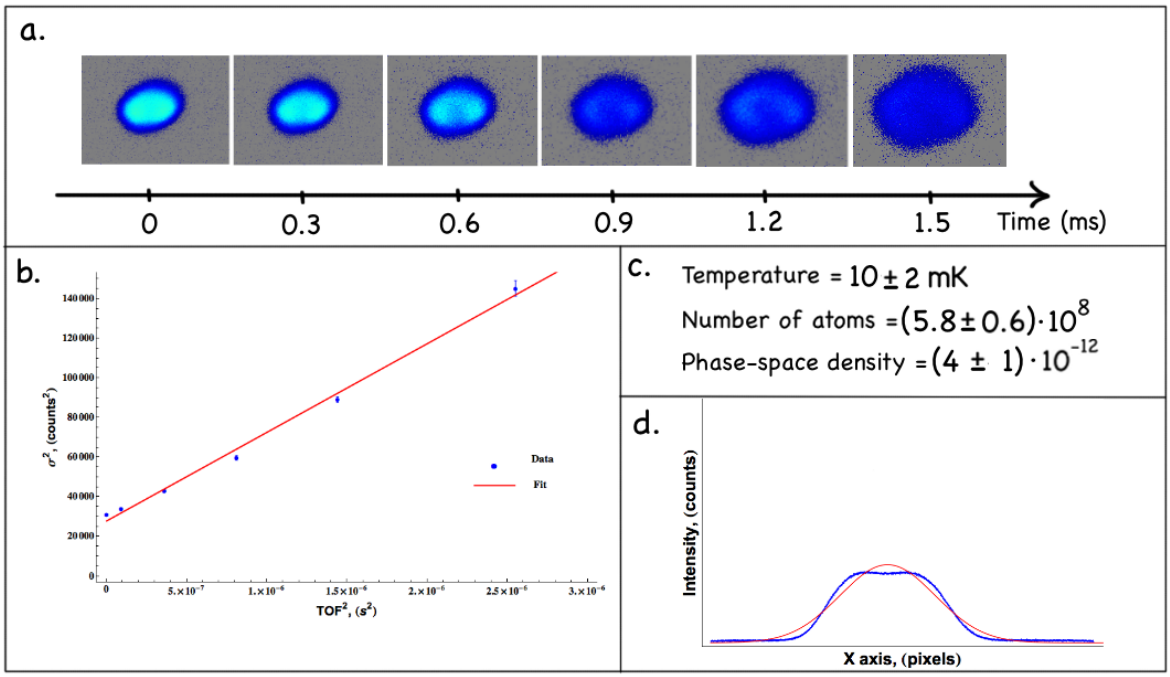

Fig. 4.6 MOT step: a. The fluorescence images of the cloud at consecutive points of time after release from the MOT. The relatively large size and fast expansion of the cloud is characteristic of the MOT cloud. **b.** The time of flight temperature measurement. **c.** Corresponding values of temperature, number of atoms and the phase-space density. **d.** The gaussian fit of the cloud.

The MOT step is optimized mainly for the number of atoms, since it puts a limit on how many atoms are cooled in subsequent steps. Also, because we are loading the trap from room temperature the detunings of the beams need to be large for the largest possible capture velocity. So, in general, the MOT cloud ends up being quite hot. In order to reduce the temperature, we add a second MOT step for 20 ms, for which we decrease the detuning of the cooling beam to -1.3Γ and increase the magnetic field gradient to 7.5 G/cm. As a result the cloud gets compressed and cooled more efficiently through Doppler cooling since closer to resonance the rate of scattering, R_{scat} is much higher. The atomic cloud right after the endMOT step has $(5.6 \pm 0.7) \times 10^8$ atoms [2] at a temperature of about 450 ± 90 μK with a phase-space density of $(3 \pm 1) \times 10^{-7}$.

[2] The drop in atom number is consistent even with a systematic error of 5% that we observe

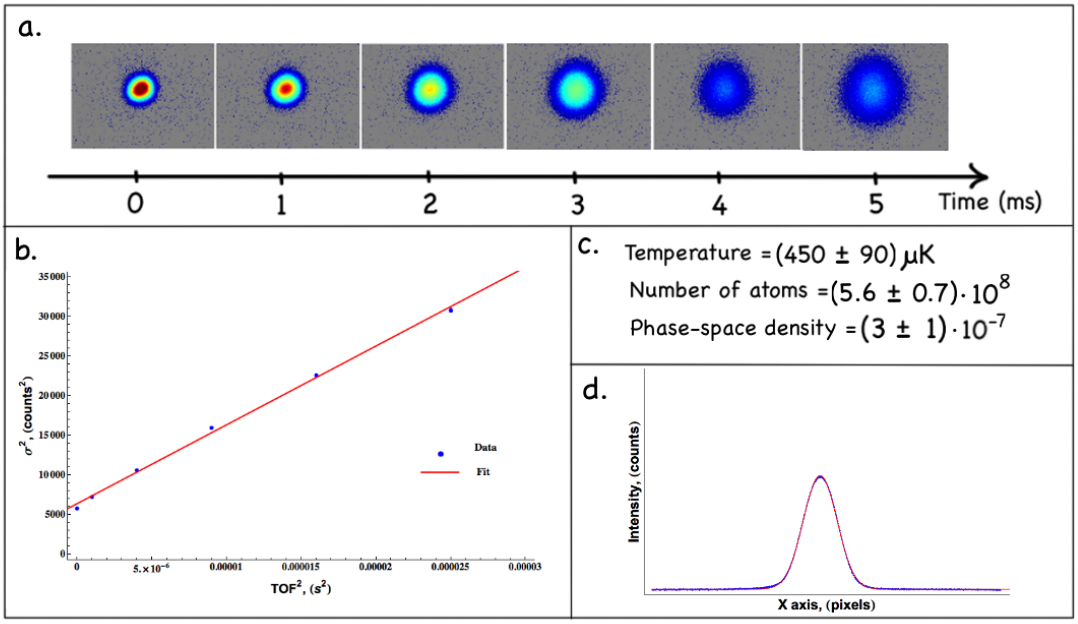

Fig. 4.7 endMOT step: a. The fluorescence images of the cloud at consecutive points of time after release from the endMOT step. **b.** The time of flight temperature measurement. **c.** Corresponding values of temperature, number of atoms and the phase-space density. **d.** The gaussian fit of the cloud.

Gray Molasses

The final stage of cooling before transferring atoms into a magnetic trap is gray molasses. The capture velocity of this mechanism is quite low so it is useful to pre-cool the cloud to the lowest possible temperature. In our experiment, we use a compressed MOT step for 4 ms described in the paper by Salomon et al. [34], which uses the gray molasses mechanism. For the CMOT we use the D1 cooling beam at detuning 6.48Γ and D2 repump beam of 0.3Γ, keeping magnetic field at 7.5G/cm. Here, atoms undergo "gray molasses"-like cooling since the magnetic field is not large enough to completely destroy the dark state, but kept in the trap because of the position-dependent force due to B field.

Similarly, the results of the temperature and atom number measurements are presented in Figure 4.8. After the CMOT, there is no loss of atoms, and the cloud is cooled down to 75 ± 10 μK with a phase-space density of $(3 \pm 1) \times 10^{-6}$. It is worth noting that the temperature of the cloud is twice as cold as reported in [34], and it is significantly below the Doppler limit for ^{39}K, $T_D = 145\mu$K.

Finally, for the gray molasses technique we turn off the magnetic field gradient and use

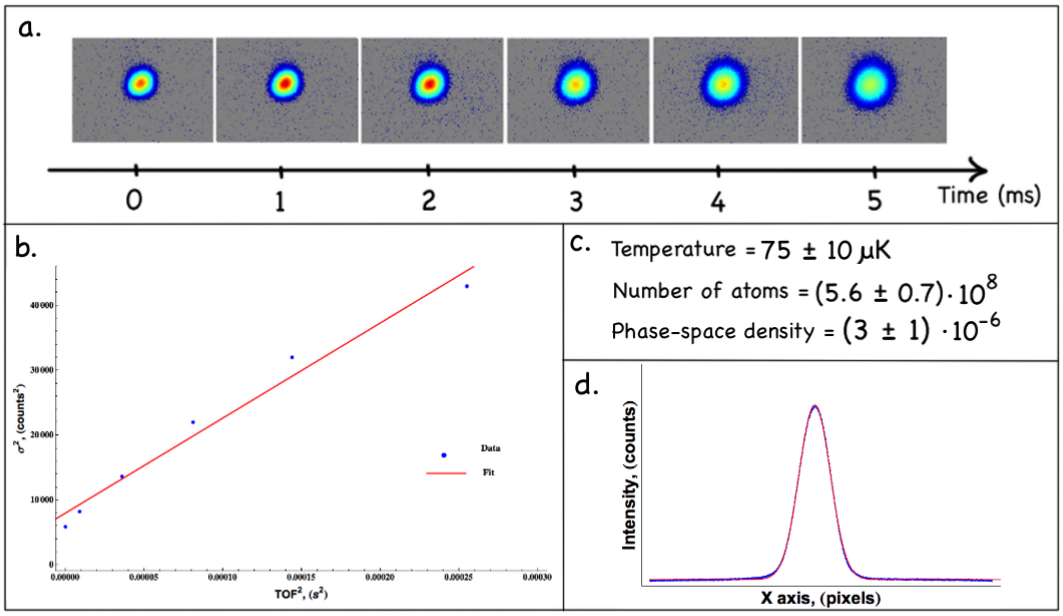

Fig. 4.8 CMOT step: a. The fluorescence images of the cloud at consecutive points of time after release from the CMOT step. **b.** The time of flight temperature measurement. **c.** Corresponding values of temperature, number of atoms and the phase-space density. **d.** The gaussian fit of the cloud.

only D1 light for 5ms. In the process of the optimization, the parameters used were δ, the relative detuning between the cooling and repump beams, and Δ_{1C}, the detuning of the cooling beam. As described in Salomon et al. [34] and Rajalakshmi et al. [29], we found the ratio of 3 : 1 of intensities of cooling and repump beams to be the most efficient for cooling. During the optimization we faced no problems with conserving the number of atoms as long as the initial capture velocity was made large by using high initial intensities of light. For optimal cooling effect, the intensities of cooling and repump beams are gradually reduced, while maintaining the 3:1 ratio as indicated in Table 4.1. The main quantity we were minimizing for was the temperature.

The plot of temperature as a function of δ and Δ_{1C} is shown in Figures 4.9 and 4.10 respectively. Both graphs have shapes closely resembling the ones obtained by Salomon et al. and Rajalakshmi et al. The δ dependence has an asymmetric Fano-like shape, with the deepest cooling achieved at 0.54MHz and strong heating for δ just above it. The sharpness of the cooling feature is characteristic of the resonance of the Raman transition. We believe the reason for the resonance being at $\delta \neq 0$ is the background magnetic fields, which shift

the energy levels so that the two-photon resonance for the Raman transition occurs at non-zero relative detuning of the beams. Further tuning of the compensation field could bring the resonance closer to $\delta = 0$ and, possibly, improve the lowest achievable temperature. The Δ_{1C} is plotted by keeping $\delta = 0.54$MHz. We found the dependence of temperature on Δ_{1C} to be quite flat up to $\Delta_{1C} \approx 2.5\Gamma$. As we get closer to 0, strong heating can be observed. This could be explained by a reduction of the dipole force, hence the Sisyphus cooling, as the detunings decrease.

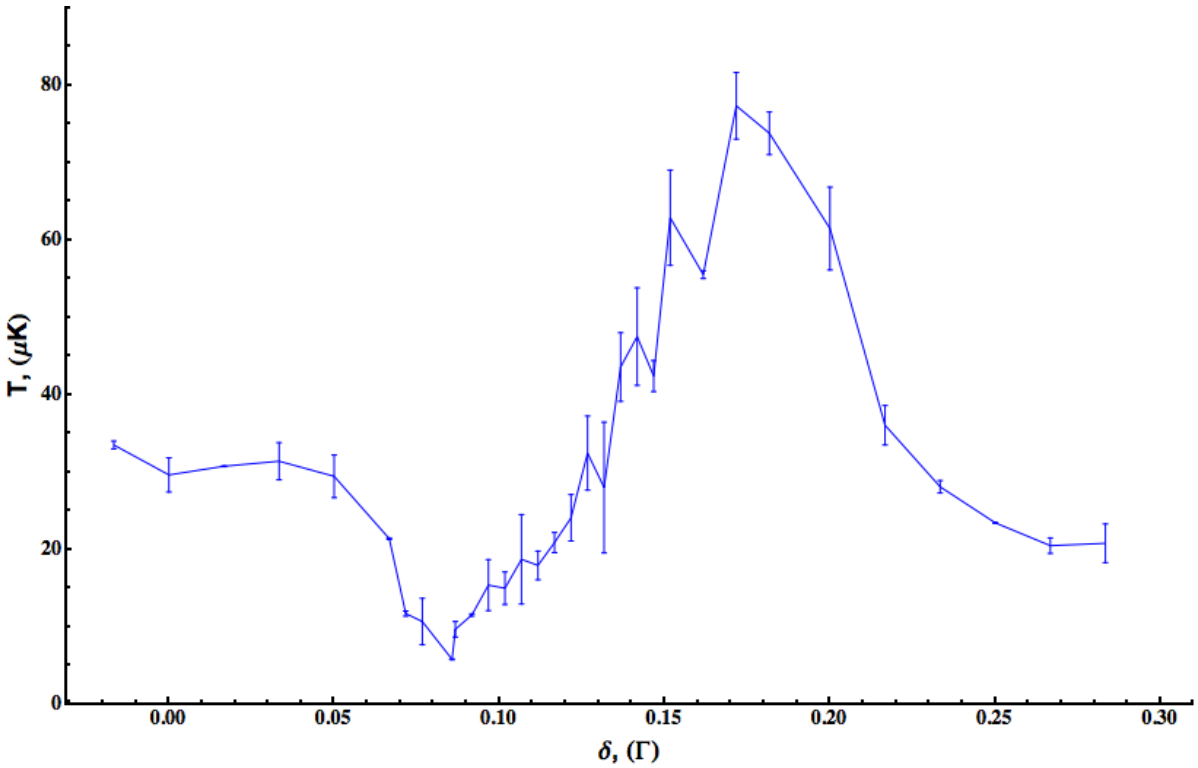

Fig. 4.9 The dependence of temperature of the cloud after gray molasses on the relative detuning δ for a fixed $\Delta_{1C} = 6.48\Gamma$. The deepest cooling is achieved at 0.54MHz corresponding to two-photon resonance. Errors are calculated from averaging over ten sets of data.

In our experiment, the lowest temperature of $\sim 5 \pm 1$ μK and a phase-space density of $(9 \pm 3) \times 10^{-5}$ after the gray molasses step was achieved for δ=0.54 MHz = 0.09 Γ and Δ_{1C} = 38.8 MHz = 6.48 Γ. The best combination of δ and Δ_{1C} is affected heavily by the variations of the amplitude of light produced by the AOM at different frequencies, so the values we achieved are strongly biased towards our experimental setup. The temperature and atom number measurements are displayed in Figure 4.11.

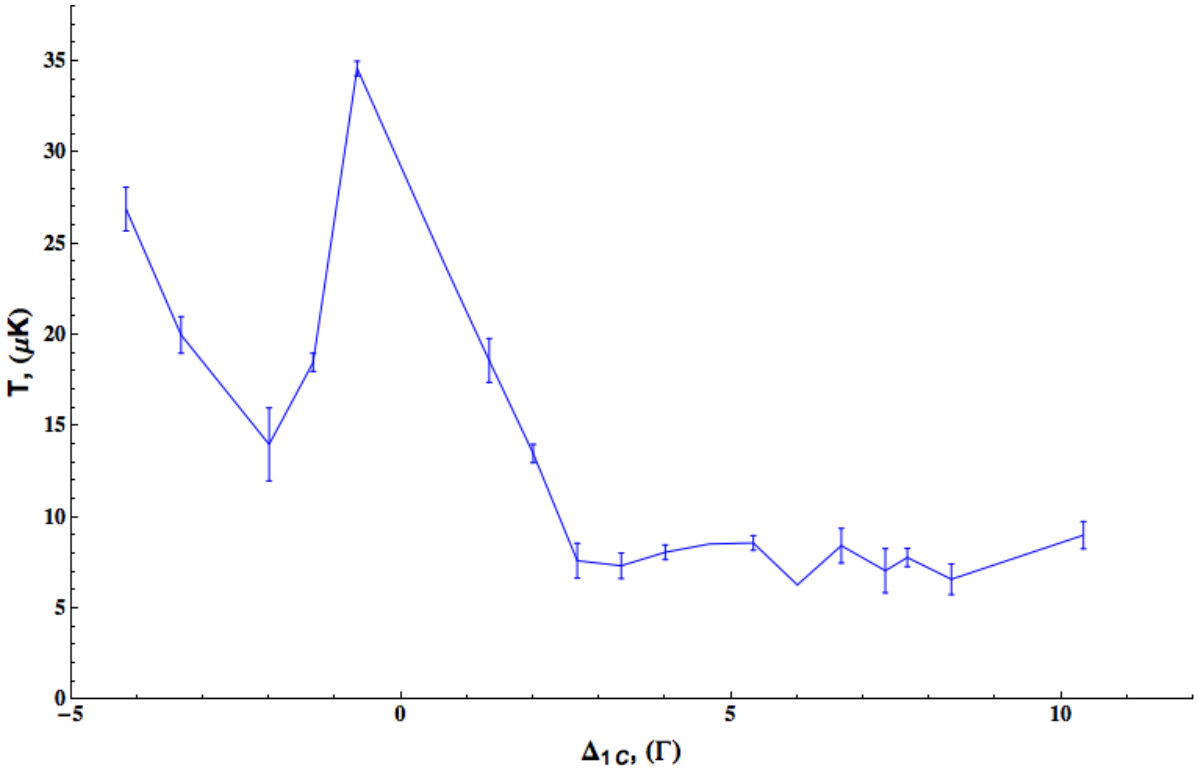

Fig. 4.10 The dependence of temperature of the cloud after gray molasses on the detuning of the cooling beam, Δ_{1C}, for a fixed $\delta = 0.09\Gamma$. It is clear that the cooling is efficient for broad values of Δ_{1C} above 2 Γ. Errors are calculated from averaging over ten sets of data.

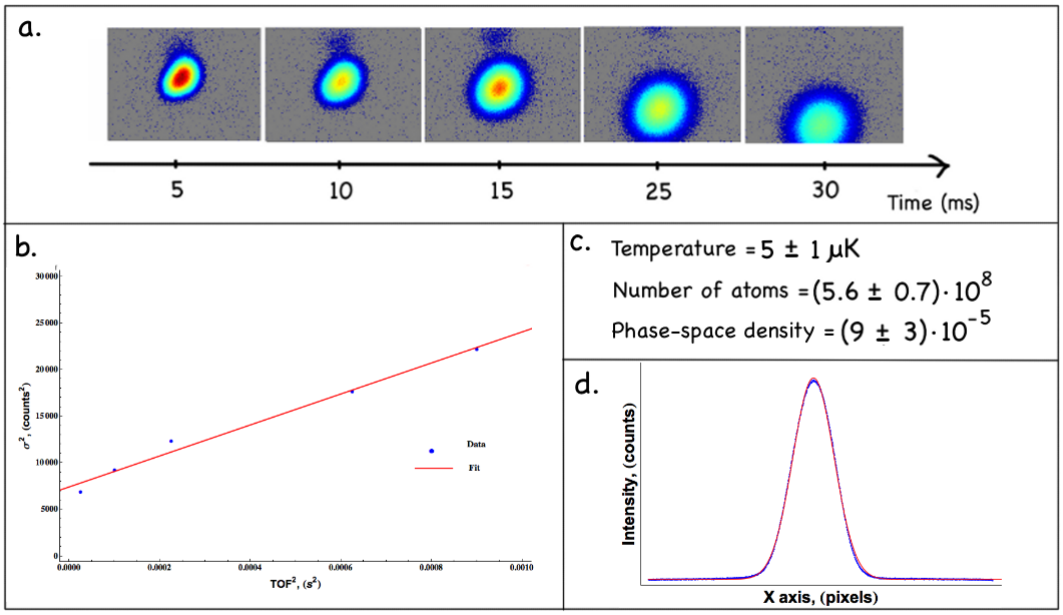

Fig. 4.11 Gray molasses: a. The fluorescence images of the cloud at consecutive points of time after gray molasses. **b.** The time of flight temperature measurement. **c.** Corresponding values of temperature, number of atoms and the phase-space density. **d.** The gaussian fit of the cloud.

Sequence Step	Duration/ Timescale	D1C Detuning Γ	D1C Intensity I_{sat}	D1R Detuning Γ	D1R Intensity I_{sat}	D2C Detuning Γ	D2C Intensity I_{sat}	D2R Detuning Γ	D2R Intensity I_{sat}	B field gradient (G/cm)
MOT	20s	-	-	-	-	-6.2	3.8	-2.0	3.5	4.5
endMOT	20ms	-	-	-	-	-1.3	3.8	-2.0	3.5	7.5
CMOT	4ms	6.48	5.1	-	-	-	-	0.3	0.4	7.5
GM	0ms	6.48	4.12	6.57	1.38	-	-	-	-	-
	4ms		1.43		0.47	-	-	-	-	
	5ms		0.83		0.27	-	-	-	-	
Optical Pumping	50μs	2.3	4.12	2.4	1.38	-	-	-	-	-
Magnetic trap	0ms	-	-	-	-	-	-	-	-	12.8
	200ms									25.6

Table 4.1 Parameter of the experimental sequence

5

Current Work

At time of writing, the work on the system continues towards achieving a BEC. In this chapter, I will discuss the steps following the cooling sequence described in Chapter 3 and 4. Some of them, including optical pumping, magnetic trapping and atom transfer, have already been successfully accomplished. Others are a work in progress, e.g. evaporative cooling and optical trapping.

5.1 Magnetic trapping

As mentioned before, our quadrupole magnetic coils have a multi-functional purpose. Aside from providing the field gradient necessary for the MOT mechanism, the coils are used for capturing atoms in a pure magnetic trap and transferring them to the science cell.

Magnetic trapping of atoms is based on the interaction between the B-field and the magnetic dipole μ of an atom. For energy shifts much smaller or bigger than the hyperfine splitting, the atom experiences an energy shift due to a Zeeman effect

$$U = g_{\mathrm{F}}\mu_{\mathrm{B}}m_{\mathrm{F}}|B_{\mathrm{z}}| \tag{5.1}$$

where g_{F} is a Lande g-factor, μ_{B} is a Bohr magneton, m_{F} is the z component of F, and B_z is the z component of the field. The energy only depends on the magnitude of the magnetic field, since, as the magnetic dipole moment moves it aligns itself to the B field. From the energy shift due to the B field, we can find the force acting on an atom

$$\boldsymbol{F} = -\nabla U = -g_{\mathrm{F}}\mu_{\mathrm{B}}m_{\mathrm{F}}\nabla B. \tag{5.2}$$

From (5.2), it follows that any states with $g_{\mathrm{F}}m_{\mathrm{F}} > 0$ will be low-field seeking states. It

means these states are magnetically trappable, since they will always lower their energy by moving towards the magnetic field minimum. The g_F factors of ground states of ^{39}K are $g_{\mathrm{F}=1} = -1/2$ and $g_{\mathrm{F}=2} = 1/2$, so the trappable $|F, m_{\mathrm{F}}\rangle$ states are $|1,-1\rangle$, $|2,1\rangle$ and $|2,2\rangle$. We chose the state $|2,2\rangle$ for trapping.

After the gray molasses step is over the atoms are distributed between the various $|F=2\rangle$ and $|F=1\rangle$ Zeeman sub-levels. To trap the highest number of atoms, the optical pumping technique is used to transfer the atoms into the state $|2,2\rangle$. First, a constant magnetic field of a few Gauss is applied to the cloud (using one coil) to split the degeneracy of the magnetic sub-levels (again using the Zeeman effect) and specify a quantization axis. Then we use the D1 Cooling and Repump circularly-polarized beams, σ^+ with respect to the quantization axis, to pump atoms into the $|2,2\rangle$ state. The mechanism relies on the fact that σ^+ only drives transitions with $\Delta m_F = +1$, where spontaneous decay obeys the usual selection rules $\Delta m_F = 0, \pm 1$. After many cycles atoms will start getting stuck at the $|2,2\rangle$ state, since it is both a *stretched state* - m_F is at its maximal value, and a *dark state* - due to a lack of a $|m_F+1\rangle$ state it doesn't interact with light.

In the experimental sequence, the detunings of the D1 Cooling and Repump beams we use are 2.3 Γ and 2.4 Γ respectively. These are non-zero due to the Zeeman energy shifts. The optical pumping step lasts 50 μs, after which all lights are turned off and the magnetic field gradient of 12.8 G/cm is abruptly turned on and ramped up to 25.6 G/cm in 200 ms. With the D1 line optical pumping, we are able to trap almost 100% of atoms cooled in the sequence. The trapping efficiency is much higher than after the optical pumping with D2 light that is used on our old ^{39}K machine. This is due to a better hyperfine structure resolution and fewer excited states of the D1 line in comparison to the D2 line. Even though gray molasses cool atoms down to 5 μK, the optical pumping and compression due to the magnetic field heats the atoms up. As a result, the temperature in the magnetic trap is about 38 μK. The results of the temperature and number of atoms measurements are shown in Figure 5.1. The cloud in the trap is not compressed homogeneously. As can be seen from the image of the cloud at t =0, the magnetic field compresses atoms along the y axis more than along x axis. The value of the phase space density is given by averaging the peak densities along x and y axes.

The lifetime of the the cloud in the trap (in the MOT chamber) was measured to be ~9.6 s using the exponential decay function, $N = N_o e^{-\frac{t}{\tau}}$, as shown in Figure 5.2

After the atoms are confined in the magnetic trap, the electric signal turns the track on and the quadrupole coils together with the confined atoms travel down the vacuum system to the science cell. We were able to successfully transfer atoms from the MOT chamber to the science cell and back, which indicates a good lifetime of the cloud and low temperatures.

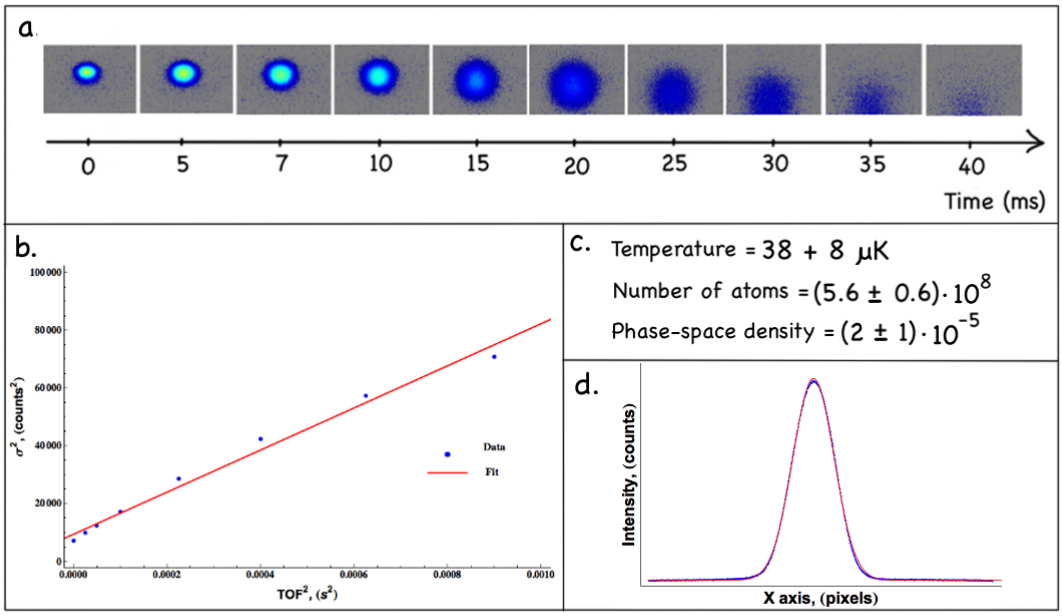

Fig. 5.1 Magnetic Trap: a. The fluorescence images of the cloud at consecutive points of time after release from the magmatic trap. **b.** The time of flight temperature measurement. **c.** Corresponding values of temperature, number of atoms and phase-space density. **d.** The gaussian fit of the cloud.

It is important to note one serious problem of the Magnetic trap, which so far hasn't caused any issues, but is a potential threat to the number of atoms in the trapped gas. In optical pumping we were very careful about transferring all of the atoms in a $|2,2\rangle$ state. However, in the trap atoms can transition into other Zeeman states, some of which are untrappable, which will cause atoms to escape the trap and be lost. This becomes an issue at the center of the quadrupole trap where $B_o = 0$. Here, without a magnetic field axis to precess about, the atoms lose orientation and can undergo so called Majorana spin flips into high-field seeking states and leave the trap. The other way to think about it is, as we get closer to $B_o = 0$ the Zeeman splittings of magnetic sub-levels become really small, which creates opportunity for atoms to jump out of $|2,2\rangle$ state. This is a problem not only because of the losses of the atoms in the trap but also due to the heating of the cloud, since the atoms closest to the center of the magnetic trap tend to be the coldest ones in the cloud. For the transfer of the cloud this issue is not as significant, but to sustain further cooling it might become a problem, since colder atoms undergo Majorana flips at a higher rate. If necessary, the atoms in the science cell will be transferred into a so-called Quadrupole-Ioffe configuration magnetic trap [14], which has a

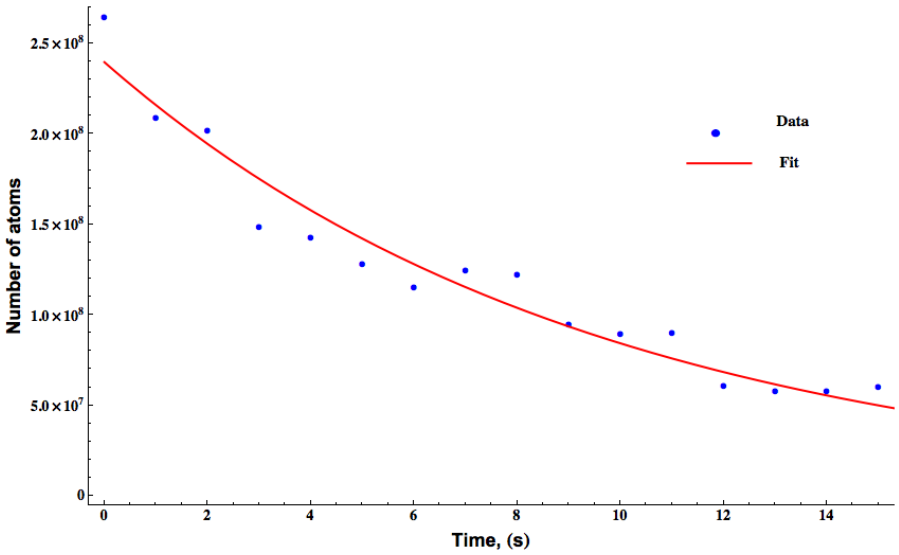

Fig. 5.2 The decay of the atomic cloud in a magnetic trap (in the MOT chamber) as a function of time. The fit function is $N = N_o e^{-\frac{t}{\tau}}$, with $\tau = 9.6$s.

non-zero trap minimum.

5.2 Work in progress

Right now work is going on the two main steps towards achieving the BEC:

- **Evaporative Cooling**

  Before being transferred into the Optical trap, atoms have to undergo further cooling in a magnetic trap by "evaporating" the cloud using the RF light. The mechanism somewhat resembles cooling a cup of tea by blowing off the hot steam. In the magnetic trap, atoms which have higher kinetic energy are located on the edges of the trap. In a quadrupole trap, the magnetic field at the edges is higher, which results in higher Zeeman shift. So by applying an RF light of a right frequency it is possible to transfer to untrappable states atoms preferentially located on the outside of the trap. This way the hottest atoms leave the trap and remaining bunch re-thermalizes to a new, lower temperature. The limitation of this cooling technique is, basically, the initial number of atoms. As long as there are atoms, it is possible to kick out hotter ones and cool the cloud. Again, even evaporative cooling of ^{39}K is not trivial. The efficiency of evaporative cooling and re-thermalization of atoms depend on the scattering length, which is quite small for potassium. It is necessary to use Feshbach resonances to increase the scattering length of ^{39}K by a factor of 100 and continue the evaporation after. In order to access Feshbach resonances, a homogenous magnetic field is required. This is one of the reasons why we cannot complete the evaporative cooling stage to the condensation in a inhomogeneous magnetic trap.

- **Optical Dipole Trap**

  The optical dipole trap (ODT) is a tool that utilizes a strong dipole force at very large detunings to optically confine atoms. We use a red-detuned optical trap to attract atoms to the maximum potential of the field. The great advantage of the optical trap is its state independence, i.e. insensitivity towards magnetic sub-levels. The ODT allows us to transfer pre-cooled atoms in the trap, use a homogenous magnetic field to increase scattering length via Feshbach resonances, and finish evaporative cooling at high efficiency. It is important to note that usually it is not viable to transfer atoms directly into the optical trap without evaporative cooling in the magnetic trap stage, due to shallow depth of the optical potential. So to conserve the maximum number of atoms we plan to transfer atoms into the optical trap after pre-cooling to about a few μK. The evaporative cooling in the ODT happens by decreasing the intensity of the trap, which gradually decreases the depth, therefore the temperature of the trapped atoms.

6

Conclusion

In this thesis, I described the working steps and results of building an ultracold atoms experiment for trapping ^{39}K. Our new experimental setup is a robust machine, which maintains an ultra high vacuum environment and allows sophisticated manipulation of external and internal degrees of freedom of atoms through interaction with an electromagnetic field. It is capable of cooling atoms by eight orders of magnitude from room temperature in the MOT chamber alone. We are currently working on completing the cooling sequence in the science cell by evaporative cooling and reaching the critical temperature of the BEC transition. To finalize the experiment, a spatial light modulator will be set up to create a uniform box potential and a magnetic field, generated by Feshbach coils, will be used to tune the interaction strength between atoms. Our group will continue efforts on finishing and optimizing the system to even higher performance.

The uniqueness and great advantage of our ultracold atoms experiment is an extreme versatility in terms of research possibilities. For a Hamiltonian of a many-body quantum system, the tunable interactions, provided by ^{39}K, will give a degree of control over the interaction part H_{int}. Additionally, the SLM will provide flexible geometries of the optical potential, resulting in variable H_{pot}. Moreover, even though my work was concentrated on condensing bosonic ^{39}K, the system is capable of working with fermionic ^{40}K and ^{87}Rb species with the addition of the corresponding laser frequencies. These combined features will open doors to a myriad of opportunities for new science. I hope the experiment will serve many years of research to our lab, and this written work will provide a source of reference for students that will be taking on the completion of this project. I tried to provide overview of experiences, limited by the maximum length of the thesis, from the perspective of a new student just coming out of an Undergraduate degree. I hope it will be useful as a reference for beginners even outside of our lab.

Appendix A

Measurement procedure

A.1 Fluorescent Imaging

The optimization of the cooling and trapping sequence required measuring the number of atoms and temperature of the cloud at particular points of the sequence. For this reason we set up a simple fluorescent imaging procedure. The six beam configuration of the MOT setup is used to shine resonant Cooling and Repump beams of the D2 line on the atoms, which causes atoms to fluoresce in all directions. The fluorescent light is gathered by a *Pixelfly pco* digital camera in a combination with a 50 mm plano-convex focusing lens, *Thorlabs LA1131*. To image the cloud, we take two pictures: one of the atoms and one of the background. By subtracting the second image from the first, we reduce the irregularities of the background that appear in the image. The data from the camera is processed and saved on the PC by a Matlab program made by Alex Gaunt. The stored image data is analyzed to obtain the number of atoms and temperature of the cloud using a program written in Mathematica.

It's worth noting that even though the main imaging sequence is done on a Pixelfly camera, other light detectors have been useful for peripheral tasks and initial setup of our system. For example, we found it very useful to have a video camera *Sony Camcorder DCR-SR45*, which is sensitive to infrared light, for live monitoring of the MOT's shape. Also, a photo diode is quite convenient for observing the loading of the trap and size of the cloud for sufficiently slow-changing processes.

A.2 Number of atoms

All of the image analysis is based on fitting a gaussian distribution to the intensity profile of the fluorescent light. The gaussian profile, $e^{-\frac{x^2}{2\sigma^2}}$, is a suitable fit for our clouds, since the quadrupole magnetic field combined with red-shifted cooling beams of the MOT encourage a harmonic shape.

Once the cloud is fitted with a gaussian[1], we have information about the width of the cloud, σ (in pixels), and the maximum height of the gaussian, $A_{\max}$ (in camera counts). First, we calculate the integral of the 2D gaussian, which gives the total amount of counts the CCD recorded, $C_{\text{total}} = \sqrt{2\pi}\sigma \cdot A_{\max}$. To convert the total number of counts to the number of photons CCD detected, we multiply C_{total} by the camera's conversion coefficient (for our camera $f \approx 25.3$ photons/count), which incorporates the quantum efficiency of the CCD. The product $C_{\text{total}} \cdot f$ gives the number of photons the camera detected from the cloud, but in order to find the number of atoms we need to know the number of photons emitted by the cloud. The total number of photons can be found by factoring in the solid angle, s, that we are detecting from. Finally, since we know how many photons an atom emits per unit of time, $1/\Gamma$, and the exposure time during imaging, t_{exp}, we can find the number of atoms

$$N = f\frac{4\pi R^2}{s}\frac{C_{total}}{t_{exp}\Gamma} \tag{A.1}$$

where R is the distance from the camera lens to the approximate center of the cloud.

A.3 Temperature

The temperature measurement was conducted using a Time of Flight (TOF) method. It is based on measuring the change in size of the cloud after a period of time in free expansion. We know that initially atoms have a gaussian shape in position space with a width σ_0. The velocity distribution of the cloud has a Maxwell-Boltzmann distribution. Approximately, the velocity profile of the cloud is $e^{\frac{mv^2}{2k_{\text{B}}T}}$ or $e^{\frac{mx^2}{2t^2k_{\text{B}}T}}$ in position space, which is a gaussian with a width $\sigma_1 = \sqrt{\frac{k_{\text{B}}Tt^2}{m}}$. Free expansion of the atomic cloud would correspond to a convolution of the initial distribution of the atoms in position space with the Maxwell-Boltzmann profile, which gives the final distribution of the cloud in position space that is also a gaussian with a width σ_2. The widths of the three gaussian distributions involved in the calculations are

[1] for optimization of the cooling and trapping sequence I used 1D gaussian fit, assuming that the cloud is symmetric. The 2D fit could be an improvement for accuracy of our measurements.

connected by

$$\sigma_0^2 + \sigma_1^2 = \sigma_2^2. \tag{A.2}$$

Both σ_0 and σ_2 could be found from imaging the atoms before and after time of flight t. This will yield σ_1, from which we can calculate the temperature

$$T = \frac{(\sigma_2^2 - \sigma_0^2)m}{k_B t^2} = \frac{\sigma_1^2 m}{k_B t^2}. \tag{A.3}$$

To achieve reliable values of temperature, we take images of the atoms after several times of flight. Then the plot of σ^2 vs t^2 gives a straight line with gradient

$$Gradient = \frac{T k_B}{m}. \tag{A.4}$$

The resulting best fit lines are shown on Figures 4.6, 4.7, 4.8, 4.11, and 5.1. It is worth noting that since the σ is in pixels and not in meters, it needs to be multiplied by the magnification of the imaging setup and the size of a pixel in the camera.

A.4 Phase-space density

The phase-space density was calculated using the peak density of the cloud. To find the peak density, n_0, we use:

$$N = \int_{-\infty}^{\infty} n_0 e^{-\frac{r^2}{2\sigma^2}} 4\pi r^2 dr = (2\pi)^{\frac{3}{2}} n_0 \sigma^3 \tag{A.5}$$

where N is the total number of atoms in the cloud and σ is a width. From the image analysis we know N (see A.2) and σ, so the peak density is

$$n_0 = \frac{N}{(2\pi)^{\frac{3}{2}} \sigma^3} \tag{A.6}$$

The thermal de Broglie wavelength of the atom is

$$\lambda_D = \sqrt{\frac{2\pi\hbar^2}{m k_b T}} \tag{A.7}$$

Using both n_0 - a measure of the volume one atom occupies in the position space, and λ_D^3 - a measure of the volume one atom occupies in phase-space, the phase-space density can be

found from

$$\rho = \lambda_D^3 n_0 \tag{A.8}$$

A.5 Absorption Imaging

We have successfully used fluorescent imaging during optimization of the system. However, the final imaging setup on the science cell side will be done using absorptive imaging, which is the most common technique in the cold atoms experiments. This method relies on attenuation of an incident beam as a result of being partially absorbed by the atomic sample. The shadow of the cloud will be recorded using the same CCD of the digital camera we used for the fluorescence. The spatially varying intensity profile is a function of cloud's spatially varying optical density. The optical density integrated along the propagation axis of the imaging beam will give the density distribution of the cloud.

Appendix B

Tables

B.1 BEC species

1995	1998	2000	2001	2003	2005	2007	2009	2010	2011	2012
^{87}Rb [2]	^{1}H [18]	^{85}Rb [8]	^{4}He [30, 33]	^{133}Cs [42]	^{52}Cr [22]	^{39}K [32]	^{40}Ca [25]	^{86}Sr [36]	^{164}Dy [26]	^{168}Er [1]
^{23}Na [9]			^{41}K [28]	^{174}Yb [38]			^{84}Sr [10, 37]			
^{7}Li [6]										

Table B.1 Atomic species that have been condensed by 15/06/2014 [39]

B.2 Current carrying magnetic coils

Coil	Wire-OD (mm)	Turns	Dimension-ID (cm)
MOT/Transport	ø4.0	10×4	ø5.1
Feshbach	ø4.0	7×2	ø7.0
Compensation Coils for MOT	ø1.0	15	ø9.0

Table B.2 Coils used in the system so far

References

[1] K Aikawa, A Frisch, M Mark, S Baier, A Rietzler, R Grimm, and F Ferlaino. Bose-Einstein Condensation of Erbium. *Phys. Rev. Lett. 108, 210401*, 2012.

[2] M Anderson, J Ensher, M Matthews, C Wieman, and E Cornell. Observation of bose-einstein condensation in a dilute atomic vapor. *Science*, 269(5221):198–201, 1995.

[3] A Aspect, E Arimondo, R e a1 Kaiser, N Vansteenkiste, and C Cohen-Tannoudji. Laser cooling below the one-photon recoil energy by velocity-selective coherent population trapping. *Physical review letters*, 61(7):826, 1988.

[4] G Audi, A Wapstra, and C Thibault. The ame2003 atomic mass evaluation:(ii). tables, graphs and references. *Nuclear Physics A*, 729(1):337–676, 2003.

[5] D Boiron, a Michaud, P Lemonde, Y Castin, C Salomon, S Weyers, K Szymaniec, L Cognet, and a Clairon. Laser cooling of cesium atoms in gray optical molasses down to 1.1 microK. *Physical review. A*, 53(6):R3734–R3737, June 1996.

[6] C.C. Bradley, C.A. Sackett, J.J. Tollett, and R.G. Hulet. Evidence of Bose-Einstein Condensation in an Atomic Gas with Attractive Interactions. *Phys. Rev. Lett.*, 75(9):1687–1691, 1995.

[7] Robert Campbell. *Thermodynamic properties of a Bose gas with tuneable interactions*. PhD thesis, 2011.

[8] S Cornish, N Claussen, J Roberts, E Cornell, and C Wieman. Stable 85Rb bose-einstein condensates with widely tunable interactions. *Phys. Rev. Lett.*, 85(9):1795–8, August 2000.

[9] K B Davis, M Mewes, M R Andrews, N J Van Druten, D S Durfee, D M Kurn, and W Ketterle. Bose-Einstein Condensation in a Gas of Sodium Atoms. *Phys. Rev. Lett.*, (November):3969–3973, 1995.

[10] Y. de Escobar, P. Mickelson, M. Yan, B. DeSalvo, S. Nagel, and T. Killian. Bose-Einstein Condensation of Sr84. *Phys. Rev. Lett.*, 103(20):200402, November 2009.

[11] Y. del Valle-Inclán Redondo. Part III project report: Laser cooling of 39 K and 87 Rb for trapping in a box potential. 2014.

[12] Chiara D'Errico, Matteo Zaccanti, Marco Fattori, Giacomo Roati, Massimo Inguscio, Giovanni Modugno, and Andrea Simoni. Feshbach resonances in ultracold 39 K. *New Journal of Physics*, 9(7):223–223, July 2007.

[13] Albert Einstein. *Quantentheorie des einatomigen idealen Gases*. Akademie der Wissenshaften, in Kommission bei W. de Gruyter, 1924.

[14] T Esslinger, I Bloch, and T Hänsch. Bose-einstein condensation in a quadrupole-ioffe-configuration trap. *Physical Review A*, 58(4):R2664, 1998.

[15] Sievers F N. Kretzschmar S.Wu C. Salomon Fernandes, D Rio and F. Chevy. Sub-Doppler laser cooling of fermionic K atoms in three-dimensional gray optical molasses. *EPL, 100 63001*, 2012.

[16] R Fletcher, A Gaunt, N Navon, R Smith, and Z Hadzibabic. Stability of a unitary bose gas. *Physical review letters*, 111(12):125303, 2013.

[17] C.J. Foot. *Atomic Physics*. Oxford University Press.

[18] D Fried, T Killian, L Willmann, D Landhuis, S Moss, D Kleppner, and T Greytak. Bose-Einstein Condensation of Atomic Hydrogen. *Phys. Rev. Lett.*, 81(18):3811–3814, November 1998.

[19] Alexander L Gaunt, Tobias F Schmidutz, Igor Gotlibovych, Robert P Smith, and Zoran Hadzibabic. Bose-Einstein condensation of atoms in a uniform potential. *Phys. Rev. Let 110.200406*, (d), 2012.

[20] V Gokhroo, G Rajalakshmi, R Easwaran, and C Unnikrishnan. Sub-doppler deep-cooled bosonic and fermionic isotopes of potassium in a compact 2d+–3d mot set-up. *Journal of Physics B: Atomic, Molecular and Optical Physics*, 44(11):115307, 2011.

[21] Andrew T Grier, Igor Ferrier-barbut, Benno S Rem, Lev Khaykovich, and Christophe Salomon. Λ -enhanced Sub-Doppler Cooling of Lithium Atoms in D 1 Gray Molasses. *Phys Rev. A 87, 063411*, 2013.

[22] A Griesmaier, J Werner, S Hensler, J Stuhler, and T Pfau. Bose-Einstein Condensation of Chromium. *Phys. Rev. Lett.*, 94(16):160401, April 2005.

[23] Rudolf Grimm, Paul Julienne, and Eite Tiesinga. Feshbach Resonances in Ultracold Gases. *Rev. Mod. Phys, 82, 1225*, 2010.

[24] G Grynberg and J.-Y. Courtois. Proposal for a Magneto-Optical Lattice for Trapping Atoms in Nearly-Dark States . *EPL*, 27(1).

[25] S Kraft, F Vogt, O Appel, F Riehle, and U Sterr. Bose-Einstein Condensation of Alkaline Earth Atoms: Ca40. *Phys. Rev. Lett.*, 103(13):130401, September 2009.

[26] Mingwu Lu, Nathaniel Q Burdick, Seo Ho Youn, and Benjamin L Lev. A Strongly Dipolar Bose-Einstein Condensate of Dysprosium. *Phys. Rev. Lett. 107, 190401*, pages 1–5, 2011.

[27] Karl-peter Marzlin. Interaction between atoms and light. http://physics.stfx.ca/~pmarzlin/lectures/al0203/marzlin-atome-licht-engl.pdf, 2003.

[28] G Modugno, G Ferrari, G Roati, R J Brecha, a Simoni, and M Inguscio. Bose-Einstein condensation of potassium atoms by sympathetic cooling. *Science (New York, N.Y.)*, 294(5545):1320–2, November 2001.

[29] Dipankar Nath, R Kollengode Easwaran, G Rajalakshmi, and C S Unnikrishnan. Quantum interference-enhanced sub-Doppler cooling of ^{39} K atoms in gray molasses. *Phys. Rev. A 88,053407*.

[30] F. Pereira Dos Santos, J. Léonard, Junmin Wang, C. Barrelet, F. Perales, E. Rasel, C. Unnikrishnan, M. Leduc, and C. Cohen-Tannoudji. Bose-Einstein Condensation of Metastable Helium. *Phys. Rev. Lett.*, 86(16):3459–3462, April 2001.

[31] D. Rio Fernandes, F. Sievers, N. Kretzschmar, S. Wu, C. Salomon, and F. Chevy. Sub-Doppler laser cooling of fermionic 40 K atoms in three-dimensional gray optical molasses. *EPL (Europhysics Letters)*, 100(6):63001, December 2012.

[32] G. Roati, M. Zaccanti, C. D'Errico, J. Catani, M. , a. Simoni, M. Inguscio, and G. Modugno. ^{39}K Bose-Einstein Condensate with Tunable Interactions. *Phys. Rev. Lett.*, 99(1):010403, July 2007.

[33] A Robert, O Sirjean, a Browaeys, J Poupard, S Nowak, D Boiron, C I Westbrook, and A Aspect. A Bose-Einstein condensate of metastable atoms. *Science (New York, N.Y.)*, 292(5516):461–4, April 2001.

[34] G Salomon, L Fouche, P Wang, A Aspect, P Bouyer, and T Bourdel. Gray molasses cooling of 39K to a high phase-space density. *EPL*, 104(6), 2013.

[35] R Smith, R Campbell, N Tammuz, and Z Hadzibabic. Effects of interactions on the critical temperature of a trapped bose gas. *Physical review letters*, 106(25):250403, 2011.

[36] S Stellmer, M Tey, R Grimm, and F Schreck. Bose-Einstein condensation of ^{86}Sr. *Phys. Rev. A 10.1103*, 2010.

[37] S Stellmer, M Tey, B Huang, R Grimm, and F Schreck. Bose-Einstein Condensation of Strontium. *Phys. Rev. Lett.*, 103(20):200401, November 2009.

[38] Y Takasu, K Maki, K Komori, T Takano, K Honda, M Kumakura, T Yabuzaki, and Y Takahashi. Spin-Singlet Bose-Einstein Condensation of Two-Electron Atoms. *Phys. Rev. Lett.*, 91(4):040404, jul 2003.

[39] Naaman Tammuz. *Thermodynamics of ultracold ^{39}K atomic Bose gases with tuneable interactions*. PhD thesis, 2011.

[40] S. Thomas. Part III project report: Sub-Doppler Laser Cooling of Potassium Atoms. 2014.

[41] H Wang, PL Gould, and WC Stwalley. Long-range interaction of the k-39 (4s)+ k-39 (4p) asymptote by photoassociative spectroscopy. 1. the og (-) pure long-range state and the long-range potential constants. *Journal of Chemical Physics*, 106(19):7899–7912, 1997.

[42] Tino Weber, Jens Herbig, Michael Mark, Hanns-Christoph Nägerl, and Rudolf Grimm. Bose-Einstein condensation of cesium. *Science (New York, N.Y.)*, 299(5604):232–5, January 2003.

[43] M. Weidemuller, T. Esslinger, M. A. Ol'shanii, A Hemmerich, and T.W. Hansch. A Novel Scheme for Efficient Cooling below the Photon Recoil Limit . *Europhys. Lett*, 109, 1994.